AD-A038 918 NAVAL SURFACE WEAPONS CENTER DAHLGREN LAB VA F/G 20/4
AERODYNAMICS OF TACTICAL WEAPONS TO MACH NUMBER 3 AND ANGLE OF --ETC(U)
FEB 77 F G MOORE, R C SWANSON

UNCLASSIFIED NSWC/DL-TR-3584 NL

1 OF 1
AD A038918

END

DATE FILMED
5-77

NSWC/DL TR-3504

AERODYNAMICS OF TACTICAL WEAPONS TO MACH NUMBER 3 AND ANGLE OF ATTACK 15° PART I – THEORY AND APPLICATION

by
FRANK G. MOORE
ROY C. SWANSON, Jr.
Warfare Analysis Department

FEBRUARY 1977

NAVAL SURFACE WEAPONS CENTER
DAHLGREN, VIRGINIA 22448
SILVER SPRING, MARYLAND 20910

NAVAL SURFACE WEAPONS CENTER
DAHLGREN LABORATORY
Dahlgren, Virginia
22448

D. M. Agnew, Jr., Capt., USN
OIC and Assistant Commander

J. H. Mills, Jr.
Associate Technical Director

NSWC/DK-TR-3584

UNCLASSIFIED

SECURITY CLASSIFICATION OF THIS PAGE (When Data Entered)

REPORT DOCUMENTATION PAGE

READ INSTRUCTIONS BEFORE COMPLETING FORM

1. REPORT NUMBER: TR-3584
2. GOVT ACCESSION NO.
3. RECIPIENT'S CATALOG NUMBER
4. TITLE (and Subtitle): AERODYNAMICS OF TACTICAL WEAPONS TO MACH NUMBER 3 AND ANGLE OF ATTACK 15° deg. PART I - THEORY AND APPLICATION
5. TYPE OF REPORT & PERIOD COVERED: Final Rept.
6. PERFORMING ORG. REPORT NUMBER
7. AUTHOR(s): Frank G. Moore, Roy C. Swanson, Jr.
8. CONTRACT OR GRANT NUMBER(s): F32323
9. PERFORMING ORGANIZATION NAME AND ADDRESS: Naval Surface Weapons Center (DK-21), Dahlgren Laboratory, Dahlgren, Virginia 22448
10. PROGRAM ELEMENT, PROJECT, TASK AREA & WORK UNIT NUMBERS
11. CONTROLLING OFFICE NAME AND ADDRESS
12. REPORT DATE: Feb[illegible]1977
13. NUMBER OF PAGES: 87 (12 75 p.)
14. MONITORING AGENCY NAME & ADDRESS (if different from Controlling Office)
15. SECURITY CLASS. (of this report): UNCLASSIFIED
15a. DECLASSIFICATION/DOWNGRADING SCHEDULE

16. DISTRIBUTION STATEMENT (of this Report)

Approved for public release; distribution unlimited.

17. DISTRIBUTION STATEMENT (of the abstract entered in Block 20, if different from Report)

DDC RECEIVED MAY 2 1977 A

18. SUPPLEMENTARY NOTES

19. KEY WORDS (Continue on reverse side if necessary and identify by block number)

Tactical weapons	Roll damping
Aerodynamic predictions	Pitch damping
Dynamic derivatives	Magnus

20. ABSTRACT (Continue on reverse side if necessary and identify by block number)

Several theoretical and empirical procedures are combined to form a useful design tool for computing static and dynamic aerodynamics on missiles, projectiles, and rockets. The Mach number and angle-of-attack range over which the method is applicable are $0 \leq M_\infty \leq 3$ and $0 \leq \alpha \leq 15°$, respectively. Body and wing geometries can be quite general in that pointed or blunt nose bodies and sharp or blunt leading edge wings can be assumed. Computed results for several configurations compare well with experimental and

(see back)

DD FORM 1 JAN 73 1473 EDITION OF 1 NOV 65 IS OBSOLETE

S/N 0102-LF-014-6601

UNCLASSIFIED

SECURITY CLASSIFICATION OF THIS PAGE (When Data Entered)

391 598

(20)

other analytical results. The computer program is cost effective as it costs less than ten dollars per Mach number to compute the lift, drag, pitching moment, magnus moment, roll damping moment, and pitch damping moment of a typical wing-body shape on the CDC 6700 computer. Thus, a reasonably accurate dynamic stability analysis and performance estimates can be made for most tactical weapons up to Mach number 3 and angle of attack 15° without wind tunnel tests. Future efforts will be directed towards increasing the Mach number capability to 6, angle of attack to 180°, and incorporating air-breathing configurations into the analysis.

FOREWORD

This work is being conducted to provide a design tool for use in estimating the aerodynamics of tactical weapons. This allows one to predict performance and to conduct a static and dynamic stability analysis in the preliminary and intermediate design stages without costly and time consuming wind tunnel tests. Support for the work was provided by the Naval Sea Systems Command under SEATASK 35A-501/090-1/UF 32-323-505. Continuation of this effort in FY 77 and beyond will be supported jointly by Naval Sea Systems Command, Naval Air Systems Command, Office of Naval Research and Army Missile Command.

This report was reviewed and approved by Mr. H. P. Caster, Head, Exterior Ballistics Division.

Released by:

R. A. NIEMANN, Head
Warfare Analysis Department

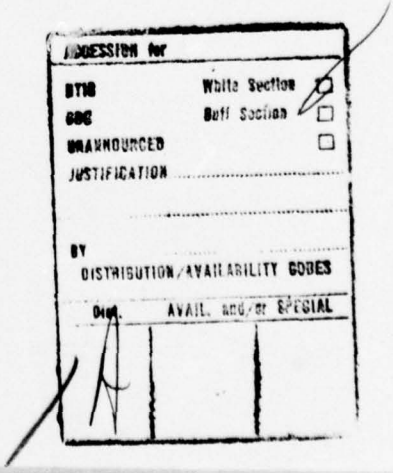

CONTENTS

LIST OF ILLUSTRATIONS

LIST OF ILLUSTRATIONS (Continued)

INTRODUCTION

Quite often the aerodynamicist, when he works with or near a design group, is faced with the task of estimating such important design parameters as range, static margin, maneuverability, dynamic stability, time to half amplitude, etc., for a given configuration. Once the design engineer obtains the data he is seeking, the next question the aerodynamicist must answer is "how can I improve the configuration so its aerodynamic properties are better"? Ultimately, an iteration cycle will probably be made in which several different configurations will be considered before the two or three most optimum candidates are chosen for further study. The important point to be made here is that for each of the above configurations, static aerodynamics (lift, drag, and pitching moment), and dynamic aerodynamics (roll damping, pitch damping, and magnus moment) must be estimated before questions concerning such things as range, maneuverability and flying qualities can be addressed.

To obtain the above set of aerodynamic coefficients, the engineer can go one of three directions: he can conduct wind tunnel tests which will be costly and time consuming and probably produce results which are more accurate than warranted for preliminary and intermediate designs, he can perform hand calculations using handbook techniques[1] and applicable experimental data but not have a good accuracy estimate of the results, or he can develop a computer program based on analytical techniques which is efficient and produces accuracies on the order of ±10 percent for most configurations. The latter alternative, although being more costly and time consuming initially, is the best approach for long term use and is the procedure which is followed in this work.

To be of practical use for tactical weapons, the theory must compute aerodynamics for the Mach number and angle of attack range of most missiles and projectiles, that is, $0 \leqslant M_\infty \leqslant 3$ and $0 \leqslant \alpha \leqslant 15°$, respectively. Also, quite general body and wing geometries must be considered. This arises from the fact that projectile noses may be pointed, truncated, or spherically blunt. Another contributing factor to the complex projectile geometries is the high setback forces at launch which means the wings and canards must be quite thick to survive the initial high "g" loads. Moreover, there may be two ogives on the nose (in the case of a fuze or blunt seeker) and a boattail present for drag reduction purposes. Figure 1 illustrates the general type of tactical weapon geometries that are encountered on nonairbreathing configurations. By designing a computer program to handle such complex geometries most missile and projectile configurations can be considered.

I. Guided Missile/Projectile (Nonairbreathing)

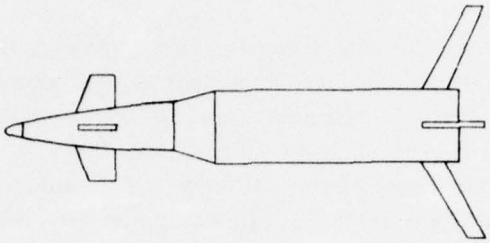

Geometry

a) Body – Nose can be pointed, blunt, or truncated with discontinuities along surface, with boattail or flare allowed.

b) Wing – Leading and trailing edge can be sharp or blunt with general modified double wedge or biconvex airfoil sections and up to two sets of lifting surfaces allowed.

II. Guided Missile (Airbreathing)

Geometry same as for nonairbreathing case except inlets added to body or wing.

III. Spin Stabilized Projectiles, Bombs, Rockets, Other Ordnance

Geometry no more general than that already considered for guided missiles.

Figure 1. Tactical Weapon Configuration Requirements

Several works existed previously which could fulfill portions of the present goal of a general aerodynamic prediction program, but none of which was satisfactory in its entirety. The most notable of these is that due to Woodward.[2] Woodward uses perturbation theory to compute the pressure distribution on wing-body combinations in subsonic and supersonic flow. However, the bodies must be pointed and the wing leading edge sharp. Also, he does not calculate the base and skin-friction drag or the nonlinear angle of attack effects. Moreover, no consideration is given to transonic flow or to the computation of the dynamic derivatives. Consideration was given to an approach such as that followed by Woodward and others for use in the present analysis to calculate static aerodynamics on tactical weapons. However, the

panel methods, which are currently in use by many scientists in the field, tend to work quite well for predicting lift and pitching moment but have limited accuracy in predicting drag for Mach numbers up to 2.5 or 3.0 and cone angles to 25°. Since drag is at least as important as lift for most tactical weapon performance characteristics, a different approach was followed for wing-body static aerodynamics.

Another method available for calculating aerodynamics on wing-body configurations is that of Saffell, et al.[3] This procedure computes static aerodynamics on low aspect ratio missile configurations. Its applicability to general aspect ratio configurations is thus questionable, particularly at small α. Furthermore, drag was calculated by handbook techniques[1] and is also quite inaccurate at small α. Again, no attention was given to the dynamic derivatives.

The other method of practical use in projectile work is the all empirical GE "Spinner" program.[4] This program computes all six aerodynamic coefficients so a dynamic stability analysis can be conducted on a spin-stabilized projectile without going to the wind tunnel. Its short comings are its lack of attention to guided weapons and limited use in body alone design due to its empirical nature. That is, effects of nose bluntness, ogive shape, boattail shape, or other discontinuites in slope cannot be estimated in detail. On the other hand, it does give total force predictions which are reasonably accurate on spin stabilized rounds which are similar in shape to the empirical data base.

To summarize the above state-of-the-art in aerodynamic prediction, it is fair to say there are several analytical or empirical methods available to compute a particular force or moment in a given Mach number regime. However, these methods have not been combined together to form a useful design tool, allowing one to not only estimate aerodynamics accurately, but to conduct static and dynamic stability analysis or trajectory simulations on a given configuration over the Mach number range from 1 to 3 and angle of attack range from 0 to 15°. It is the purpose of the present work to provide such a tool.

ANALYSIS

STATIC AERODYNAMICS

The static aerodynamics have been computed previously and the reader is referred to References 5 through 9 for the details of that portion of the present work. Only a synopsis of that work will be included here for continuity purposes.

Body Alone Aerodynamics

A summary of the various methods for computing body alone aerodynamics appears in Figure 2. All the methods are standard in the literature (References 10 through 15) with the exception of the empirical schemes derived for transonic lift and wave drag and the combined Newtonian-perturbation theory for calculating nose wave drag in supersonic flow. The combined Newtonian-perturbation theory was developed so reasonable results for static aerodynamics could be obtained at low supersonic Mach numbers for blunt nosed configurations. Comparisons with experimental data indicate this method accurately predicts pressure coefficients and total force coefficients down to supersonic Mach numbers of 1.2.

COMPONENT \ MACH NUMBER REGION	SUBSONIC	TRANSONIC	SUPERSONIC
NOSE WAVE DRAG	——	Wu and AOYOMA PLUS EMPIRICAL	2nd ORDER VAN DYKE PLUS MODIFIED NEWTONIAN
BOATTAIL WAVE DRAG	——	Wu and AOYOMA	2nd ORDER VAN DYKE
SKIN FRICTION DRAG	VAN DRIEST II		
BASE DRAG	EMPIRICAL		
INVISCID LIFT and PITCHING MOMENT	EMPIRICAL	Wu and AOYOMA PLUS EMPIRICAL	TSIEN 1st ORDER CROSSFLOW
VISCOUS LIFT and PITCHING MOMENT	ALLEN and PERKINS CROSSFLOW		

Figure 2. Methods Used to Compute Body Alone Aerodynamics

Wing and Interference Aerodynamics

The methods used to compute the wing alone and interference aerodynamics are listed in Figure 3. Again the methods are standard in the literature (References 16 through 22) except for the empirical techniques used for wing-body interference, trailing edge separation drag, and body base pressure drag caused by tail fins and except for the theoretical computation of wing wave drag in supersonic flow. For the details of these techniques, the reader is again referred to either References 7 or 9.

COMPONENT \ MACH NUMBER REGION	SUBSONIC	TRANSONIC	SUPERSONIC
INVISCID LIFT AND PITCHING MOMENT	LIFTING SURFACE THEORY	EMPIRICAL	LINEAR THEORY
WING-BODY INTERFERENCE	SLENDER BODY THEORY AND EMPIRICAL		LINEAR THEORY, SLENDER BODY THEORY & EMPIRICAL
WING-TAIL INTERFERENCE	LINE VORTEX THEORY		
WAVE DRAG	——	EMPIRICAL	LINEAR THEORY + MODIFIED NEWTONIAN
SKIN FRICTION DRAG	VAN DRIEST		
TRAILING EDGE SEPARATION DRAG	EMPIRICAL		
BODY BASE PRESSURE DRAG CAUSED BY TAIL FINS	EMPIRICAL		

Figure 3. Methods Used to Compute Static Wing Alone and Interference Aerodynamics

ROLL DAMPING MOMENT

The body alone roll damping moment is estimated using the same procedure as the "Spinner" program.[4] That is, if one knows C_{ℓ_p} as a function of Mach number for a given configuration, then

$$C_{\ell_p} = (C_{\ell_p})_1 \frac{\ell}{\ell_1}$$

where the subscript represents known data. This estimate should prove reasonable so long as the data available is for a configuration of similar dimensions to the configuration for which data is required.

For a wing-body configuration, the wing completely dominates the roll damping moment so it is of primary concern to have a good estimate of the wing alone roll damping.

For supersonic and subsonic flow calculations, the wing is assumed to be thin so that small perturbation theory can be employed for flow-field calculations. In addition, the wing is assumed to have zero camber with aeroelastic effects being small. In transonic flow, empirical methods are used for roll damping calculations. Body interference is estimated using slender body theory. Tail fin to tail fin interference is zero unless the non-dimensional spin $pd/2V_\infty$ is high enough so the shed vortices impinge on an adjacent fin.

The individual methods used for calculating the wing roll damping moment coefficient derivatives in subsonic, supersonic, and transonic flow, along with the interference effects, are discussed below.

Subsonic Flow ($M_\infty < M_{crit}$)

The small perturbation equation for three-dimensional steady flow is:[16]

$$\beta^2 \phi_{x_0 x_0} - \phi_{y_0 y_0} - \phi_{z_0 z_0} = 0 \qquad (1)$$

where the subscripts x_0, y_0, z_0 indicate partial differentiation and where the velocity potential, ϕ, is related to the perturbation velocities by

$$\phi_{x_0} = u/V_\infty, \quad \phi_{y_0} = v/V_\infty, \quad \phi_{z_0} = w/V_\infty . \tag{2}$$

The boundary conditions are that the flow is undisturbed at an infinite distance from the surface, is tangential to the surface, and is continuous at the wing trailing edge. Mathematically, these boundary conditions can be treated in respective order by:

$$u = v = w = 0 \quad \text{as} \sqrt{x_c^2 + y_c^2 + z_c^2} \to \infty \tag{3a}$$

$$\vec{V}_m \cdot \nabla F = 0 \tag{3b}$$

$$\begin{aligned} u_u[(x_0)_{TE}, y_0, z_0] &= u_\ell[(x_0)_{TE}, y_0, z_0] \\ v_u[(x_0)_{TE}, y_0, z_0] &= v_\ell[(x_0)_{TE}, y_0, z_0] \\ w_u[(x_0)_{TE}, y_0, z_0] &= w_\ell[(x_0)_{TE}, y_0, z_0] \end{aligned} \tag{3c}$$

The boundary condition (3c) is simply a definition of the Kutta condition which requires the velocity at the trailing edge to be continuous from the upper to lower surfaces. If the equation of the surface is defined as $z_0 = F(x_0, y_0)$, then (3b) implies

$$\frac{w(x_0, y_0)}{V_\infty} \approx \phi_{z_0} = \frac{\partial F(x_0, y_0)}{\partial x_0} = \alpha(x_0, y_0) \tag{4}$$

The angle of attack, $\alpha(x_0,y_0)$ can be expressed as

$$\alpha(x_0,y_0) = \alpha_0 + py_0/V_\infty + q(x_0 - x_{ref})/V_\infty \tag{5}$$

where α_0 is the angle of attack of the wing planform, py_0/V_∞ is the induced angle of attack at a point y_0 on the wing span due to a steady roll rate p, and $q(x_0 - x_{ref})/V_\infty$ is the induced angle of attack at a point x_0 along the wing chord due to a constant pitch rate q.

Equation (1) is a linear partial differential equation so that superposition of solutions is valid. Therefore, for roll damping calculations, one can set $\alpha_0 = q = 0$ in Equation (5) so the boundary condition of interest is

$$\phi_{z_0} = py_0/V_\infty \tag{6}$$

Equation (1) can be simplified somewhat by using Göthert's extension to the Prandtl Glauert transformation. This transformation is equivalent to

$$\left.\begin{aligned} x &= x_0/\beta_1 \\ y &= y_0 \\ z &= z_0 \\ \phi(x,y,z) &= \phi(x_0,y_0,z_0) \end{aligned}\right\} \tag{7}$$

where $\beta_1 = \sqrt{1 - M_\infty^2}$. Equation (1) then simplifies to

$$\phi_{xx} + \phi_{yy} + \phi_{zz} = 0 \tag{8}$$

Thus, the compressible flow on a wing of given geometry can be solved for by affinely relating the wing to another wing with the properties of Equation (7), and solving for the flow field on the new wing at $M_\infty = 0$. Once this is done, the pressure coefficient at any point on the wing is:[16]

$$C_P(x_0, y_0, z_0) = -2\phi_x/\beta \tag{9}$$

The solution to Equation (8) can be shown to be:[17]

$$\phi(x,y,z) = \frac{1}{8\pi}\int_S\int \frac{\Delta C_p(x_1,y_1)}{(y-y_1)^2+z^2}\, z\left[1+\frac{x-x_1}{\sqrt{(x-x_1)^2+(y-y_1)^2+z^2}}\right] dx_1\, dy_1 \tag{10}$$

where $\Delta C_P = C_{P_\ell} - C_{P_u}$. It is required to determine the pressure loading ΔC_P over the entire surface. Following Chadwick,[17] Equation (10) is first differentiated with respect to z and the limit as $z \to 0$ taken. The result is then equated to the boundary condition, Equation (6), to obtain:

$$\frac{py}{V_\infty} = \frac{1}{8\pi}\fint\int \frac{\Delta C_P(x_1,y_1)}{(y-y_1)^2}\left[1+\frac{x-x_1}{\sqrt{(x-x_1)^2+(y-y_1)^2}}\right] dx_1\, dy_1 \tag{11}$$

The cross on the y_1 integral indicates a singularity at $y = y_1$, in which case Manglers principal-value technique[16] can be applied. The details of the solution of the integral Equation (10) for $\Delta C_P(x,y)$ will not be repeated here as they are given in many references (see for example, Reference 17). Worthy of note, however, is the fact that Equation (11) is an integral equation for which the wing loading ΔC_P is to be found as a linear function of the induced angle of attack, py/V_∞.

Once the span loading $\Delta C_P(x,y)$, due to roll, is known over the entire wing, the local rolling moment coefficient at a given spanwise airfoil section, y, is

$$c_\ell = \frac{y}{c\ell_{ref}}\int_{x_{LE}}^{x_{TE}} (\Delta C_P)_p\, dx \tag{12}$$

where the subscript P indicates the loading due to a roll rate p. The total rolling moment on the entire wing is then

$$C_\ell = \frac{2}{S_{ref}}\int_0^{b/2} c c_\ell\, dy \tag{13}$$

Assuming the rolling moment is a linear function of roll rate, the roll damping moment coefficient derivative is

$$C_{\ell_P} = \frac{C_\ell}{p\ell_{ref}/2V_\infty} \tag{14}$$

Supersonic Flow ($M_\infty \geq 1.2$)

For supersonic flow past thin wings, Equation (1) is still applicable along with the associated boundary condition (3b). Since the flow is supersonic, disturbances in the flow-field are not felt upstream of the point of disturbance. Thus, the boundary condition (3a) can be modified to,

$$u(0^-,y,z) = v(0^-,y,z) = w(0^-,y,z) = 0 \tag{15}$$

where it is assumed the disturbance occurs at $x = 0$. It will be assumed the wing trailing edge is supersonic (Mach number normal to wing trailing edge is greater than one) so that the Kutta condition need not be applied. The solution to Equation (1) is:[18]

$$\phi(x_0,y_0) = -\frac{1}{\pi}\int_{S_1}\int \frac{\alpha(y_0,y_0)}{\sqrt{(x_0 - x_1)^2 - \beta^2(y_0 - y_1)^2}}\, dx_1 dy_1 \tag{16}$$

where S_1 is the wing planform. The lifting pressure coefficient, due to a constant roll rate p, is then related to the velocity potential ϕ through the relation

$$(\Delta C_P)_P = -4\phi_{x_0} \tag{17}$$

The limits of integration of Equation (16) are dependent on whether the leading edge is subsonic or supersonic. Each of these cases will be considered separately below.

Supersonic Leading Edge. By supersonic leading edge, one means the Mach number normal to the leading edge is greater than one. Referring to Figure 4, this implies the Mach line emanating from the root chord, OA, lies behind the wing leading edge. If the Mach line intersects the wing tip, as shown in Figure 4, there are five distinct disturbance regions present and hence, five different perturbation solutions. If the Mach line intersects the wing trailing edge, the disturbance created by the Mach line OA impinging on the wing tip is eliminated so that only four perturbation solutions are needed.

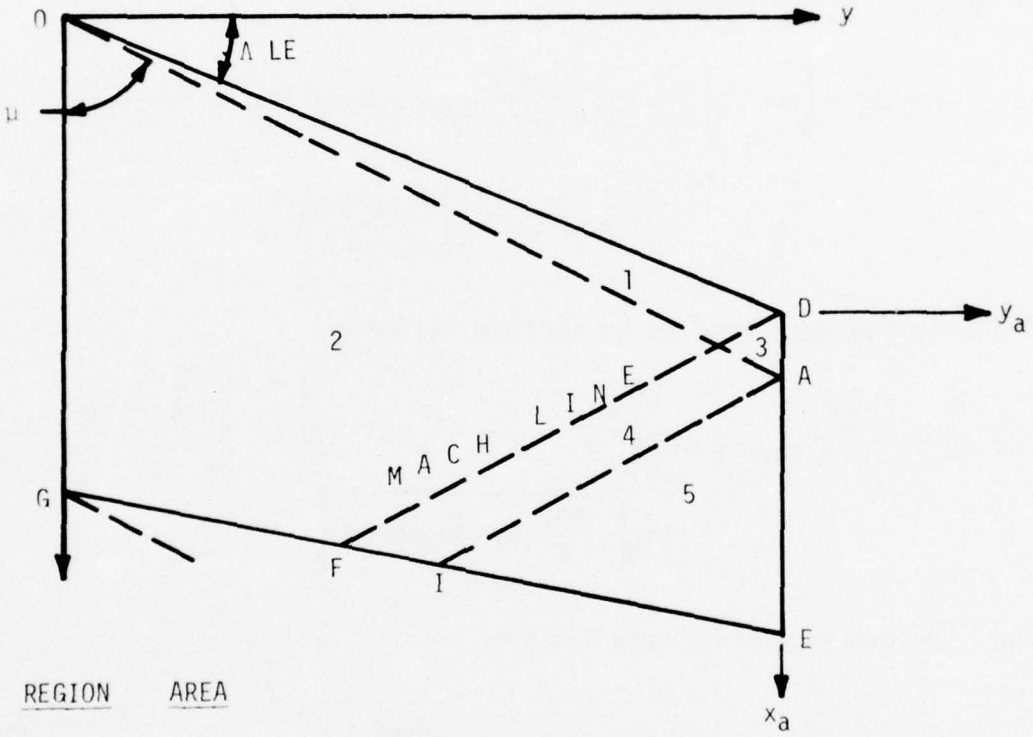

REGION	AREA
1	ODH
2	OHFG
3	AHD
4	FHAI
5	AEI

Figure 4. Flat Plate Wing Planform With Supersonic Leading and Trailing Edges; Mach Line Intersects Wing Tip

The generalized formulas for the lifting pressure distributions on a wing in steady roll are derived in Reference 21. For convenience, the final equations are repeated here. For region 1, the flow is two-dimensional and the resulting lifting pressure is

$$(\Delta C_P)_P = \left[(\Delta C_P)_P\right]_1 = \frac{4pm^2 x_0 (m^2\sigma - 1)}{\beta^2 V_\infty (m^2 - 1)^{3/2}} \tag{18}$$

In region 2, the total lifting pressure is:

$$(\Delta C_P)_P = \left[(\Delta C_P)_P\right]_2 = \frac{4pm^2 x_0}{\pi\beta^2 V_\infty (m^2 - 1)^{3/2}} \left\{(1 + m^2\sigma)\cos^{-1}\left[\frac{1 + m^2\sigma}{m(1+\sigma)}\right]\right.$$

$$\left. -(1 - m^2\sigma)\cos^{-1}\left|\left[\frac{1 - m^2\sigma}{m(1-\sigma)}\right]\right|\right\} \tag{19}$$

The induced pressure caused by the tip Mach line DF is:

$$[(\Delta C_P)_P]_3 = \frac{4pm}{\pi V_\infty \beta (m^2-1)^{3/2}} \left\{\left[\frac{mx_a}{\beta} - m^2 y_a - \frac{b}{2}(m^2 - 1)\right]\cos^{-1}\left[\frac{\frac{mx_1}{\beta} + y_a(2m + 1)}{y_a - \frac{mx_a}{\beta}}\right]\right.$$

$$\left. -2m\sqrt{-\frac{my_a}{\beta}(x_a + \beta y_a)(m + 1)}\right\} \tag{20}$$

The total lifting pressure in region 3 is then:

$$(\Delta C_P)_P = [(\Delta C_P)_P]_1 + [(\Delta C_P)_P]_3 \tag{21}$$

The lifting pressure in region 4 is a combination of that in Regions 2 and 3. Thus, in Region 4:

$$(\Delta C_P)_P = [(\Delta C_P)_P]_2 + [(\Delta C_P)_P]_3 \tag{22}$$

Again, if the Mach line OA intersects the wing trailing edge, Equations 18 through 22 allow one to determine the complete lifting pressure distribution over the wing surface. If the Mach line OA intersects the wing tip, another perturbation is induced in the flow field. The total pressure differential in region 5 is then:

$$(\Delta C_P)_P = \frac{4pm}{\pi\beta V_\infty (m^2-1)^{3/2}} \left\{ \left[\frac{mx_a}{\beta} + m^2 y_a + \frac{b}{2}(m^2+1) \right] \cos^{-1} \left(\frac{mx_a/\beta - y_a(1-2m) + b}{mx_a/\beta + y_a + b} \right) \right.$$
$$\left. -2m\sqrt{-y_a(m-1)(mx_a/\beta + my_a + b)} \right\} \qquad (23)$$

Subsonic Leading Edge. If the Mach number normal to the leading edge is less than one (and the trailing edge Mach number is greater than one), there are only two flow regions to consider. However, the solution is complicated somewhat by the leading edge singularity where the velocity goes like $1/x$.[22] Referring to Figure 5, the pressure differential of upper and lower surfaces in Region 1 is:[22]

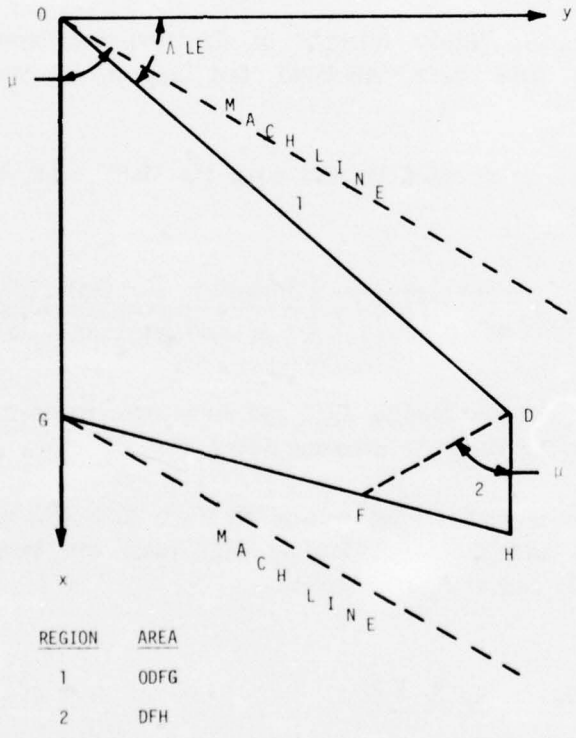

REGION	AREA
1	ODFG
2	DFH

Figure 5. Flat Plate Wing Planform With Subsonic Leading Edge and Supersonic Trailing Edge

$$(\Delta C_P)_P = \frac{2I(m)pm^2 x_0 \sigma}{\beta^2 V_\infty \sqrt{1 - \sigma^2}} \tag{24}$$

where

$$I(m) = \frac{2(1 - m^2)}{(2 - m^2)E(m) - m^2 F(m)}$$

$$E(m) = \int_0^{\pi/2} \sqrt{1 - k^2 \sin^2 \theta}\, d\theta$$

$$F(m) = \int_0^{\pi/2} \frac{d\theta}{\sqrt{1 - k^2 \sin^2 \theta}}$$

$$k = \sqrt{1 - m^2}$$

Values of the complete elliptic integrals of the first and second kind (F(m) and E(m), respectively) have been tabulated and appear in standard mathematical handbooks.

Region 2, which is affected by the wing tip Mach cone, has a lifting pressure differential given by:

$$(\Delta C_P)_P = \frac{-8pm}{\pi\beta V_\infty} \sqrt{b/2 - y} \left[\frac{3mx_0/\beta + y(1 - 2m) - b/2(1 + m)}{3(1+m)\sqrt{(1+m)(mx_0/\beta + y_0)}} \right] \tag{25}$$

For a flow with a subsonic leading edge and supersonic trailing edge, Equations (24) and (25) determine the complete pressure distribution due to a steady roll, p.

The local roll moment, total rolling moment, and roll damping moment for both the subsonic and supersonic leading edge cases can then be determined by Equations (12), (13) and (14), respectively.

Transonic Flow ($M_{fb} \leq M_\infty < 1.2$)

There are currently no simple, accurate analytical methods available for calculating transonic roll damping. With the increased emphasis on transonic

aerodynamics in the last few years, it is hoped a simple theoretical method will become available within a reasonable time frame. Until that time, one must resort to the full Navier Stokes equations of motion or empirical techniques. Since the former approach is beyond the scope of this work, the empirical approach will be followed.

Without a theoretical model to calculate transonic roll damping, it has been current practice by some engineers[23] to estimate roll damping in direct proportion to the lift. That is

$$(C_{\ell_P})_M = (C_{\ell_P})_{M=M_{fb}} \frac{(C_{N_\alpha})_M}{(C_{N_\alpha})_{M=M_{fb}}} \tag{26}$$

where the quantities C_{ℓ_P} and C_{N_α} are total configuration values. This means that if the roll damping is known at say $M_\infty = 0.8$ and C_{N_α} is known throughout the transonic speed regime, then the roll damping can be estimated according to Equation (26). This is the procedure used in the present analysis for calculating roll damping.

One of the main problems inherent in calculating transonic aerodynamics is a need to account for thickness, and in some cases, aeroelastic effects. An empirical technique proposed by Edmondson[24] to correct for thickness and aeroelastic effects on rectangular wings is

$$C_{\ell_P} = (C_{\ell_P})_{theory}(1 - t/c)^{2AR/3} \tag{27}$$

where t/c is the overall thickness to chord ratio of the wing planform. However, the present values of $(C_{\ell_P})_{theory}$ in transonic flow are calculated based on the lift curve slope which has already accounted for thickness. In addition, intuitively, one would expect a Mach number effect to be present in Equation (27), since thickness is most important in transonic flow. For these two reasons, Equation (27) was not applied in the present analysis.

Interference Effects

There are three types of interference effects which need to be examined in the process of predicting roll damping. These are the body-fin, tail fin to tail fin and

canard to tail interference effects. The first arises due to the presence of the body, the second as a result of tail shed vortices impacting another tail fin, and the third as a result of canard shed vortices impacting the tail fins.

Using slender body theory, the effect of the body has been calculated by Adams and Dugan[25] for both planar and cruciform wing-body combinations. The results of their calculations are presented in Figure 6 as a function of the parameter

$$\xi = r_b/(r_b + b/2)$$

It is seen that there is little difference between the planar and cruciform wing configuration and furthermore, that the body has little effect on the roll damping for values of ξ up to 0.4. Although these results are analytical, they have been verified qualitatively by the experimental results presented in Reference 1.

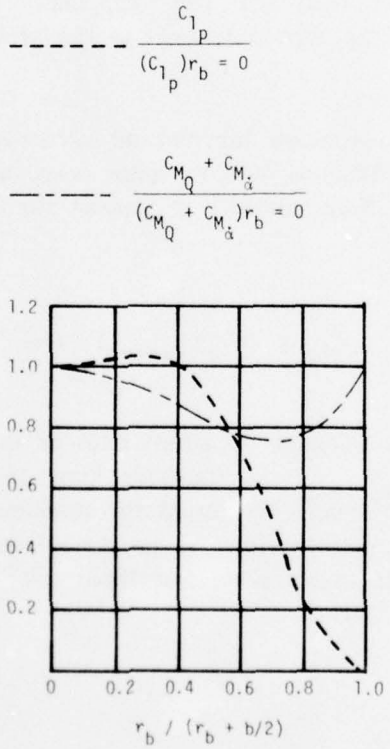

Figure 6. Effect of Body Radius on Damping in Roll and Pitch for Fixed Span

The effect of the number of fins on roll damping was at first determined using slender body theory.[27] The results indicated that the addition of fins to a missile adds to the damping in roll at a decreasing rate. However, slender body theory results are independent of Mach number. Moreover, most tactical weapons fly at Mach numbers such that the nondimensional spin $p\ell_{ref}/2V_\infty$ is so low that tail fin shed vortices do not affect other tail fins. Hence, tail fin to tail fin interference for most practical cases is zero, and is therefore neglected here.

Canard-tail interference will not be accounted for at this time. Several personnel are currently involved in estimating induced roll and it is hoped that this form of interference can be incorporated into the current methodology at some future time.

MAGNUS FORCE AND MOMENTS

There have been several analytical attempts at predicting Magnus (References 28 through 31) characteristics as a function of the main variables of interest; that is, Mach number, Reynolds number, body shape and various properties of the boundary layer. All of these methods have given some success for given conditions, but, as of yet, there is still no accurate analytical method by which one can calculate Magnus as a function of Mach number and body shape for typical projectile/missile ordnance. The latest of the theoretical attempts to predict Magnus is due to Vaughn.[31] To evaluate the capability of Vaughn's method, several projectile configurations were considered in which his method was compared with experimental data and an all-empirical prediction model "Spinner".[4] Figure 7 presents the results of these calculations. As seen in the figure, the empirical model is better for predicting Magnus than the theoretical model of Vaughn. Since neither approach does very well in general, it appears there is still much analytical work to be done before Magnus forces and moments on projectile and missile ordnance can be predicted.

Reference 32 attempted to generalize the empirical Spinner approach to incorporate boattail geometry variations in the prediction scheme. Graff[32] et al., found that one could correlate the magnus force and moment as a linear function of the Mangler variable, η, where η is defined by:

$$\eta = \left[\frac{\int_{\ell - \ell_{BT}}^{\ell} r^2 dx}{r_{ref}^2 \ell_{BT}} \right] \tag{28}$$

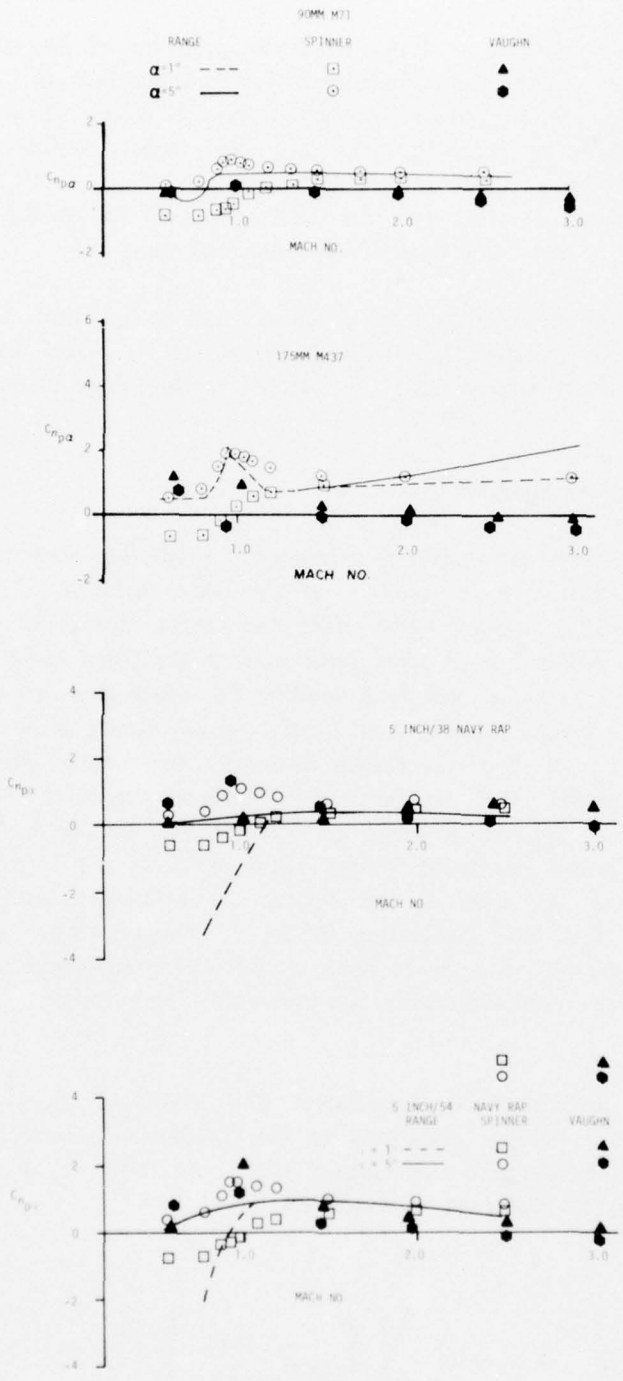

Figure 7. Magnus Moment Coefficient Derivative for Four Projectiles

which for conical boattails integrates to:

$$\eta = .58\left[1 + \left(\frac{r_b}{r_{ref}}\right) + \left(\frac{r_b}{r_{ref}}\right)^2\right]^{1/2} \tag{29}$$

An empirical scheme was thus developed which included boattail shape in addition to length in the methodology. However, when the method was compared to other prediction techniques for existing ordnance, it appeared the method of Reference 32 did not do significantly better than the Spinner technique. Since the method in Reference 32 was only for angles of attack up to 1°, the Spinner program will be used to estimate magnus effects on spin-stabilized ordnance.

For fin-stabilized weapons it will be assumed the configuration rolls slow enough so magnus effects can be neglected.

PITCH DAMPING MOMENT

There are two contributions to the damping in pitch. These are the steady state derivative C_{M_Q} (the moment coefficient due to steady pitching velocity) and the unsteady state or time dependent derivative $C_{M_{\dot{\alpha}}}$ (the moment coefficient due to a constant vertical acceleration). In order to determine the total damping of missile configurations, the damping of individual components (i.e., body, wings, and canards) is calculated, and then the wing-body interference is included.

The empirical procedure of the "Spinner" program is employed to estimate the body-alone pitch damping parameter. Thus, the quantity $C_{M_Q} + C_{M_{\dot{\alpha}}}$ for a particular body is related to the damping value for a dimensionally similar body by a function of the body length, boattail length, and center of gravity.

The lifting surfaces of missiles (canard-body-tail configurations) and fin-stabilized projectiles (body-tail configurations) generally represent the major contribution of the total damping in pitch. Therefore, it is important to have a good estimate of the wing-alone pitch damping.

For subsonic and supersonic flow calculations, once again a thin wing is assumed so that small perturbation theory is applicable. Also, as in the section Roll Damping Moment, the wing is assumed to have no camber or twist and negligible aeroelastic effects. In transonic flow, empirical methods are applied in longitudinal damping computations. The component interference effects are then approximated by assuming a slender body and using the apparent-mass method of Bryson.[33]

The individual procedures used for calculating the wing pitch damping moment coefficient derivatives in all flight regimes under consideration and the interference effects are presented in the following discussion.

Subsonic Flow ($M_\infty < M_{fb}$)

The stability derivatives C_{L_Q} and C_{M_Q} for a thin wing in subsonic flow are determined from the pressure distribution corresponding to a steady pitching rate q. In the case of incompressible flow the pressure variation is obtained by solving Equation (1), the small perturbation equation for three-dimensional steady flow, with the appropriate boundary condition. For steady state pitch damping calculations the necessary boundary condition is found by setting $\alpha_0 = p = 0$ in Equation (5). Thus,

$$\phi_{z_0} = q(x_0 - x_{ref})/V_\infty \tag{30}$$

Moreover, the pressure loading due to a constant pitch rate is realized by solving the integral equation given by Equation (11) with py/V_∞ replaced with $q(x_0 - x_{ref})/V_\infty$. The resulting solution is the wing loading ΔC_p. Compressible subsonic calculations are based upon the incompressible solution by applying Göthert's extension to the Prandtl-Glauert rule, which is given along with the expression for the pressure coefficient C_p in Equations (7) and (9), respectively.

From the chordwise pressure distribution, the sectional moment about the axis of rotation of the wing due to q is determined, specifically,

$$c_{M_q} = \frac{1}{c\ell_{ref}} \int_{x_{LE}}^{x_{TE}} x(\Delta C_p)_q \, dx \tag{31}$$

where the quantity $(\Delta C_p)_q$ represents the loading due to a pitch rate q. The total pitching moment due to q on the entire wing is given by:

$$(C_M)_q = \frac{2}{S_{ref}} \int_0^{\frac{b}{2}} cc_{M_q} \, dy \tag{32}$$

Assuming the pitching moment is a linear function of pitch rate, the steady state pitch damping moment coefficient derivative is

$$C_{M_Q} = \frac{(C_M)_q}{\left(\frac{q\ell_{ref}}{2V_\infty}\right)} \tag{33}$$

Many of the recent developments in the field of unsteady aerodynamics (i.e., References 34 and 35) indicate that oscillatory lifting surface theory represents the most viable approach in the prediction of unsteady subsonic stability derivatives for arbitrary wing planforms. However, the computational effort required by this theory to obtain such derivatives precluded the possibility of being able to readily incorporate the technique into the present subsonic calculation scheme (steady lifting surface theory). Two-dimensional unsteady methods (i.e., References 36 and 37) for estimating $C_{L_{\dot{\alpha}}}$ and $C_{M_{\dot{\alpha}}}$, which assume small amplitude oscillations and correct for finite span effects, appear to be inadequate to handle basic wing planforms (i.e., rectangular, triangular, tapered, sweptback, etc.) for a complete aspect ratio range. Although a simple solution for $C_{M_{\dot{\alpha}}}$ in the case of a triangular wing is obtained by Tobak and Lessing in Reference 38, the mathematical intricacies associated with the method, which reduces an unsteady flow problem to an equivalent steady flow problem, prohibit similar simple solutions for other wing planforms.

In the present treatment of subsonic flow, the constant vertical acceleration derivative $C_{M_{\dot{\alpha}}}$ for the wing alone is given its steady flow value ($C_{M_{\dot{\alpha}}} = 0$). Since the primary concern here is the prediction of dynamic derivatives for tail-body or wing-body-tail configurations, this deficiency does not seriously impair the preliminary design objective. It is interesting to note the theoretical predictions of $C_{M_Q} + C_{M_{\dot{\alpha}}}$, which assume $C_{M_{\dot{\alpha}}} = 0$, for a delta wing ($AR = 2.4$) and a sweptback and tapered wing ($AR = 3$) that are presented in Figures 20 and 21. These figures are discussed in the results section.

If only small amplitude oscillations are considered (i.e., reduced frequency $\omega\ell_{ref}/2V_\infty \ll 1$), and the flow over the body is assumed to be in phase with the flow over the tail (i.e., the time required by a change in body vortex strength due to a change in angle of attack to travel to the tail is small in comparison to the period of oscillation), it is probably reasonable to assume that the unsteady derivative $C_{M_{\dot{\alpha}}}$ is approximately zero for a tail-body in subsonic flow. However, this is not the situation for a canard-body-tail configuration. In particular, the tail contribution to the damping parameter $C_{M_{\dot{\alpha}}}$ resulting from the downwash lag

phenomenon should be considered. Since there is a finite time required for the downwash discharged from a forward lifting surface to reach the tail, it can be shown[27] that the tail contribution to $C_{M_{\dot{\alpha}}}$ is given by

$$(C_{M_{\dot{\alpha}}})_T = -2\left(\frac{dC_L}{d\alpha}\right)_T\left(\frac{q'_T}{q'_\infty}\right)\left(\frac{d\epsilon}{d\alpha}\right)_T\left(\frac{x_{ref}}{\ell_{ref}}\right)_T^2 \tag{34}$$

where the subscript T means the value associated with the tail, and x_{ref} is the distance between the vehicle center of gravity and the center of pressure of the tail. The downwash variation with respect to angle of attack can be calculated from the tail effectiveness parameter. That is,

$$\left(\frac{d\epsilon}{d\alpha}\right)_T = 1 - \eta_T$$

and

$$1 - \eta_T = -\frac{C_{L_{T(V)}}}{(C_L)_{BT} - C_{L_B}},$$

where $C_{L_{T(v)}}$ is the lift coefficient for the negative lift at the tail due to the downwash induced by the wing shed vortex, $(C_L)_{BT}$ is the lift coefficient for the body-tail combination, and C_{L_B} is the lift coefficient for the body alone. Details for computing these quantities are given in Reference 7.

Supersonic Flow ($M_\infty \geq 1.2$)

The pressure loading distributions to calculate the pitch damping $C_{M_Q} + C_{M_{\dot{\alpha}}}$ are obtained by using Equation (17). To determine the perturbation velocity potential and thus ϕ_x in that equation the unsteady wave equation, which is

$$\frac{1}{a_\infty^2}\left(\frac{\partial}{\partial t} + V_\infty\frac{\partial}{\partial x}\right)^2\phi = \frac{\partial^2\phi}{\partial x^2} + \frac{\partial^2\phi}{\partial y^2} + \frac{\partial^2\phi}{\partial z^2} \tag{35}$$

and is derived from linearized small disturbance theory, is solved. On the basis of a first-order frequency solution to the above equation, an expression for the time-dependent disturbance velocity potential for a wing accelerating downward at a positive angle of attack $\dot{\alpha}t$ is given by[39]

$$\phi = \dot{\alpha}\left[\frac{M^2}{\beta^2}\,\phi_{q=1} + \left(t - \frac{M^2 x}{\beta^2 V_\infty}\right)\phi_{\alpha=1}\right]. \tag{36}$$

Using the same analysis it can also be shown that the lifting pressure (evaluated at time t = 0) is

$$\Delta C_P = \left[\frac{\dot{\alpha}}{\beta^2}\;M^2(\Delta C_P)_{q=1} - \frac{M^2 x}{V_\infty}(\Delta C_P)_{\alpha=1} - \frac{4}{V_\infty^2}\,\phi_{\alpha=1}\right] \tag{37}$$

where $\phi_{q=1}$ and $(\Delta C_P)_{q=1}$ are the perturbation velocity potential and the pressure loading, respectively, due to unit (positive) steady pitching velocity about the y-axis and where $\phi_{\alpha=1}$ and $(\Delta C_P)_{\alpha=1}$ are, analogously, the perturbation velocity potential and pressure loading, respectively, due to unit (positive) angle of attack. Thus, the unsteady flow problem is reduced to an equivalent steady flow problem, and it now remains to determine the steady quantities just mentioned in order to obtain the desired stability derivatives and pitch damping.

From the results that are given in References 40 and 41, the potential and corresponding ΔC_P due to angle of attack are readily determined for a thin wing in supersonic flow. In particular, Equation (1), which is the steady flow version of Equation (35), is solved by Evvard's source sheet method[42] using the appropriate boundary condition ($\phi_z = \alpha$). The solution is given in Equation (16). For a constant rate of pitch the solution just referred to is again applicable with the associated boundary condition ($\phi_z = qx/V_\infty$). As it has been indicated previously, the limits of integration of Equation (16) are dependent on whether the leading edge of a given wing is subsonic or supersonic.

Supersonic Leading Edge. A description of the supersonic leading edge case is given in the Supersonic Leading Edge for Roll Damping Moment. The generalized formulas for the lifting pressure distributions on a wing with a constant pitching velocity or a constant vertical acceleration are derived, except for region 5, in References 39 and 40. Referring to Figure 4, the flow in region 1 is two-dimensional, and the resulting lifting pressure is

$$(\Delta C_P)_q = [(\Delta C_P)_q]_1 = \frac{4qmx}{\beta V_\infty (m^2 - 1)^{3/2}} [m^2 - 2 + \sigma] \tag{38}$$

$$(\Delta C_P)_{\dot\alpha} = [(\Delta C_P)_{\dot\alpha}]_1 = -\frac{4\dot\alpha mx(1-\sigma)}{\beta V_\infty (m^2-1)^{3/2}} \left(\frac{m^2+1}{\beta^2}\right) \tag{39}$$

In region 2, the total lifting pressure is

$$(\Delta C_P)_q = [(\Delta C_P)_q]_2 = \frac{8qmx}{\pi\beta V_\infty} \left\{ \frac{\sqrt{1 - m^2\sigma^2}}{(m^2-1)} + \frac{(m^2-2-\sigma)}{2(m^2-1)^{3/2}} \cos^{-1} \frac{1+m^2\sigma}{m(1+\sigma)} + \frac{(m^2-2+\sigma)}{2(m^2-1)^{3/2}} \cos^{-1} \frac{1-m^2\sigma}{m(1-\sigma)} \right\} \tag{40}$$

$$(\Delta C_P)_{\dot\alpha} = [(\Delta C_P)_{\dot\alpha}]_2 = \frac{4\dot\alpha x}{V_\infty \beta^2 \pi (m^2-1)^{3/2}} \left\{ \frac{2M^2 m}{\beta} \sqrt{(1 - m^2\sigma^2)(m^2-1)} - (m^2+\beta^2) \frac{m}{\beta} \left[(1+\sigma) \cos^{-1} \frac{1+m^2\sigma}{m(1+\sigma)} + (1-\sigma) \cos^{-1} \frac{1-m^2\sigma}{m(1-\sigma)} \right] \right\} \tag{41}$$

The induced pressure caused by the tip Mach line DF, added to the contribution of region 1, yields the total lifting pressure in region 3:

$$(\Delta C_P)_q = \frac{8q}{\pi V_\infty} \left[\frac{\frac{mx_a}{\beta}(m^2-2) + y_a + \frac{b}{2}(m^2-1)}{2(m^2-1)^{3/2}} \cdot \cos^{-1} \frac{\frac{mx_a}{\beta} + (2m+1)y_a}{\frac{mx_a}{\beta} - y_a} - \frac{(1+m-m^2)}{m^2-1} \sqrt{-my_a \left(\frac{x_a}{\beta} + y_a\right)} \right] \tag{42}$$

$$(\Delta C_P)_{\dot\alpha} = \frac{4\dot\alpha}{V_\infty \beta\pi (m^2-1)^{3/2}} \left\{ [\beta(m^2 - m - 1) - m] \sqrt{-4y_a(m+1)\left(\frac{mx_a}{\beta} + my_a\right)} - \beta\left(\frac{mx_a}{\beta} - y_a\right)(m^2+1) \cos^{-1} \frac{\frac{mx_a}{\beta} + (2m+1)y_a}{\frac{mx_a}{\beta} - y_a} \right\} \tag{43}$$

The lifting pressure in region 4 is a combination of that in regions 2, 3, and 1. Thus, in region 4:

$$(\Delta C_P)_q = [(\Delta C_P)_q]_2 + [(\Delta C_P)_q]_3 - [(\Delta C_P)_q]_1 \tag{44}$$

$$(\Delta C_P)_{\dot{\alpha}} = [(\Delta C_P)_{\dot{\alpha}}]_2 + [(\Delta C_P)_{\dot{\alpha}}]_3 - [(\Delta C_P)_{\dot{\alpha}}]_1 \tag{45}$$

The total pressure differential in region 5 is

$$(\Delta C_P)_q = \frac{4q}{\pi V_\infty (m^2 - 1)^{3/2}} \left\{ \left[(m^2 - 2)\frac{mx_a}{\beta} - y_a + (m^2 - 3)\frac{b}{2} \right] \cos^{-1} \left(\frac{mx_a/\beta - y_a(1 - 2m) + b}{mx_a/\beta + y_a + b} \right) + 2(m^2 + m - 1)\sqrt{-y_a(m - 1)\left(\frac{mx_a}{\beta} + my_a + b \right)} \right\} \tag{46}$$

$$(\Delta C_P)_\alpha = \left(\frac{4\dot{\alpha}}{\beta^2} \right) \frac{M^2}{\pi V_\infty (m^2 - 1)^{3/2}} \left\{ - \left(\frac{mx_a}{\beta} + y_a + b \right) \left(1 + \frac{(m^2 - 1)}{M^2} \right) \cdot \cos^{-1} \left(\frac{mx_a/\beta - y_a(1 - 2m) + b}{mx_a/\beta + y_a + b} \right) + 2\left[(m^2 - 1)\left(1 - \frac{1}{M^2} \right) + m \right] \sqrt{-y_a(m - 1)\left(\frac{mx_a}{\beta} + my_a + b \right)} \right\} \tag{47}$$

Subsonic Leading Edge. For a wing with a subsonic leading edge the physical description is given in the Subsonic Leading Edge for Roll Damping Moment. Referring to Figure 5, the pressure differentials of the upper and lower surfaces in region 1 are[41]

$$(\Delta C_P)_q = 4q \frac{m}{\beta} \frac{G(m)}{V_\infty} \left[\frac{x(2 - \sigma^2)}{\sqrt{1 - \sigma^2}} \right] \tag{48}$$

$$(\Delta C_P)_{\dot{\alpha}} = \frac{4\dot{\alpha}}{V\beta^2} \left\{ M^2 \frac{m}{\beta} G(m) \frac{(2 - \sigma^2)}{\sqrt{1 - \sigma^2}} x - M^2 \frac{m}{\beta} \frac{xE''(m)}{\sqrt{1 - \sigma^2}} - \frac{m}{\beta} xE''(m)\sqrt{1 - \sigma^2} \right\} \tag{49}$$

where

$$G(m) = \frac{1 - m^2}{(1 - 2m^2)E(m) + m^2 F(m)} ,$$

$$E'(m) = \frac{1}{E(m)} ,$$

and the elliptic integrals E(m) and F(m) are defined after Equation (24).

Region 2, which is affected by the wing tip Mach cone, has lifting pressures given by

$$(\Delta C_P)_q = \frac{4q}{3\pi V_\infty} \left\{ \left[\frac{\frac{6mx}{\beta}(3 + 2m) + (12 + 8m + m^2)y - bm(1 + m)}{(m + 1)^2} \right] \cdot \sqrt{\frac{(m + 1)(b - 2y)}{2\left(\frac{mx}{\beta} + y\right)}} \right\} \tag{50}$$

$$(\Delta C_P)_{\dot\alpha} = \frac{4\dot\alpha}{V\beta^2} \left\{ M^2 \left[\frac{\frac{6m}{\beta}(3 + 2m) + (12 + 8m + 2m^2)y - mb(m + 1)}{3\pi (m + 1)^{3/2}} \right] \right.$$

$$\left. \cdot \sqrt{\frac{b/2 - y}{\frac{mx}{\beta} + y}} - \frac{2M^2 mx}{\pi\beta} \sqrt{\frac{b/2 - y}{(m + 1)\left(\frac{mx}{\beta} + y\right)}} - \frac{4}{\pi} \sqrt{\frac{\left(\frac{mx}{\beta} + y\right)\left(\frac{b}{2} - y\right)}{m + 1}} \right\} \tag{51}$$

For a flow with a subsonic leading edge and supersonic trailing edge, Equations (48) through (51) determine the complete pressure distribution due to steady pitching rate q and constant vertical acceleration $\dot\alpha$ ($\sim\ddot z$).

The local pitching moment due to q and the total pitching moment due to q are calculated using Equations (31) through (33). The same quantities due to $\dot\alpha$ are obtained using Equations (31) through (33) by replacing q and Q with $\dot\alpha$.

Transonic Flow ($M_{fb} \leq M_\infty < 1.2$)

The problem of no simple, accurate analytical method to estimate dynamic aerodynamic coefficient derivatives is encountered again. As in previous cases, the only viable approach consistent with the present computational cost effective objective is an empirical one.

The first step in the approximation of the transonic pitch damping is to determine the value at the force break Mach number by applying the aforementioned subsonic calculation procedure. Then, employing the empirical method discussed in Reference 7, sweep, Mach number, aspect ratio, and thickness are taken into account. That is

$$(C_{M_Q} + C_{M_{\dot{\alpha}}})_M = (C_{M_Q} + C_{M_{\dot{\alpha}}})_{M=M_{fb}} \frac{(C_{N_\alpha})_M}{(C_{N_\alpha})_{M=M_{fb}}} , \qquad (52)$$

where the quantities $C_{M_Q} + C_{M_{\dot{\alpha}}}$ and C_{N_α} are the total configuration values. Moreover, if the damping in pitch is known at the nominal force break Mach number of 0.8, and C_{N_α} is known throughout the transonic speed regime, an estimate of pitch damping in transonic flow can be made with Equation (52).

Interference Effects

As mentioned earlier, once the aerodynamic loadings on the components of a flight configuration due to a particular kind of motion are estimated, the interference effects are then determined in order to obtain the total forces and moments. An application of the apparent-mass method of Bryson[33] provides an approximation for an interference damping reduction factor, which is defined as the ratio of the pitch damping of a wing-body combination to the pitch damping of the total wing (i.e., the exposed wing panels extended through the body). The variation of this factor with respect to the nondimensionalized body radius ξ, which is defined in the Interference Effects for Roll Damping Moment, is presented in Figure 6. This figure shows a decrease in the damping of the total wing as a result of the presence of the body. Moreover, the damping reduction factor reaches a minimum of .75 at ξ equal to .71. After this factor is determined for a given configuration, the total wing-body derivatives C_{L_Q}, C_{M_Q}, $C_{L_{\dot{\alpha}}}$, and $C_{M_{\dot{\alpha}}}$ are found by adding the modified wing value to the exposed body alone contribution, where the exposed body is the section of the body beyond the apex of the wing.

When a configuration includes both forward and aft lifting surface panels, the induced damping in pitch due to wing-tail interference requires attention also. The effects of the wing shed vortices on the tail contribution to the longitudinal damping can be calculated in one of two ways:[1]

1. If there is direct interaction between the aft lifting surfaces and the vortices shed from the forward lifting surfaces ($b_w/b_T < 1.5$), the wing-tail interference is approximated by

$$\pm 2\left(\frac{x_{ref}}{\ell_{ref}}\right)^2 (C_{L_\alpha})_{w''(v)} ,$$

   where $(C_{L_\alpha})_{w''(v)}$ is the negative lift of the tail due to wing-tail interference, and x_{ref} is the distance between the vehicle center of gravity and the center of pressure of the tail. The sign of the above expression is negative if there is pure pitching motion, and it is positive if there is vertical acceleration motion.

2. If there is no such direct interaction ($b_w/b_T \geq 1.5$), the wing-tail interference is neglected.

Note, only one trailing vortex is assumed for each forward lifting surface panel.

Figure 8 summarizes the methods used for computing the dynamic derivatives.

COMPONENT \ MACH NUMBER REGION	SUBSONIC	TRANSONIC	SUPERSONIC
BODY ALONE ROLL DAMPING MOMENT	EMPIRICAL		
WING AND INTERFERENCE ROLL DAMPING	LIFTING SURFACE THEORY	EMPIRICAL	LINEAR THEORY
BODY ALONE MAGNUS MOMENT	EMPIRICAL		
WING AND INTERFERENCE MAGNUS MOMENT	ASSUMED ZERO		
BODY ALONE PITCH DAMPING MOMENT	EMPIRICAL		
WING AND INTERFERENCE PITCH DAMPING MOMENT	LIFTING SURFACE THEORY	EMPIRICAL	LINEAR THEORY

Figure 8. Methods Used to Compute Dynamic Derivative

CURRENT STATUS AND FUTURE EFFORT

The current status of the present effort to develop an aerodynamic prediction capability for tactical weapons is shown in Figure 9. As seen in the figure, aerodynamics can be estimated up to low supersonic Mach numbers ($M_\infty \leq 2.5$) and angles of attack to 20° for nonairbreathing tactical weapons.

CONFIGURATION	SUBSONIC (0-0.8)	TRANSONIC (0.8-1.2)	LOW SUPER (1.2-2.5)	HIGH SUPER (2.5-8)	LOW α (0-20)	MEDIUM α (20-60)	HIGH α (60-180)
GUIDED MISSILE NON-AIR BREATHING	✓	✓	✓		✓		
GUIDED MISSILE AIR BREATHING						N. A.	N. A.
BOMB, ROCKET, STORES	✓	✓	✓		✓		N. A.
SPIN-STABILIZED PROJECTILE	✓	✓	✓		✓	N. A.	N. A.
GUIDED PROJECTILE	✓	✓	✓		✓	N. A.	N. A.
DAMAGED CONFIGURATIONS	PORTIONS		PORTIONS			N. A.	N. A.

Figure 9. Current Status of Aerodynamic Prediction for Tactical Weapons

It appears that future tactical weapons will be designed for higher speeds, incorporating higher angles of attack for improved maneuverability. To obtain the higher speeds, airbreathing configurations appear to be one of the more attractive methods. The main thrust of the future effort will therefore be to extend the methodology to high supersonic Mach numbers for angles of attack to 180° and to also consider the airbreathing configurations.

Two other areas are also of interest for future effort. These are improving those methodologies which have been outdated in the past several years by new technology and optimization of the computer program for ease of use when the work is complete. It is envisioned these three efforts will take from 3 to 4 years, depending on the funding available in a given year, starting in fiscal year 1977. After the work is complete and documented, the computer program will be turned over to the computer programming division at NSWC/DL for maintenance, updating, and suppling to other parts of the DoD, along with their contractors.

RESULTS AND DISCUSSION

STATIC AERODYNAMICS

Three cases are presented to show comparison of the present static aerodynamics methodology with experimental data. These cases consist of a spin stabilized projectile (body-alone configuration), an unguided missile (body-tail configuration), and a complicated canard-body-tail configuration. These cases are sufficiently different and complex to test all the individual theoretical and empirical procedures of Figures 2 and 3, and to indicate typical results to be expected from the prediction of static forces and moments. For more detailed comparisons, refer to References 5 through 9.

Figure 10 gives the static aerodynamic coefficients for the improved 5"/54 projectile. The improved round has a 2.75 caliber nose and a 1.0 caliber boattail with a discarding rotating band. Excellent agreement with experimental data is obtained for the drag coefficient throughout the entire Mach number range. Fair agreement is obtained for normal force coefficient and hence pitching moment and center of pressure. The comparison for the lifting properties is Mach number dependent: in the low supersonic region the theory is consistently about 10 percent low on normal force, whereas at intermediate supersonic speeds it compares very well with experiment. The reason for this behavior is the failure of the inviscid theory to predict afterbody lift correctly at low supersonic Mach numbers. At subsonic and transonic Mach numbers, the theory does about as well as could be expected, considering the amount of empirical methodology in that region.

The second case is a 10-caliber missile with clipped delta tail fins. The experimental data are taken from Reference 43, which gives the static aerodynamics for $0.8 \leq M_\infty \leq 1.3$. Figure 11 compares theoretical drag coefficient, normal force

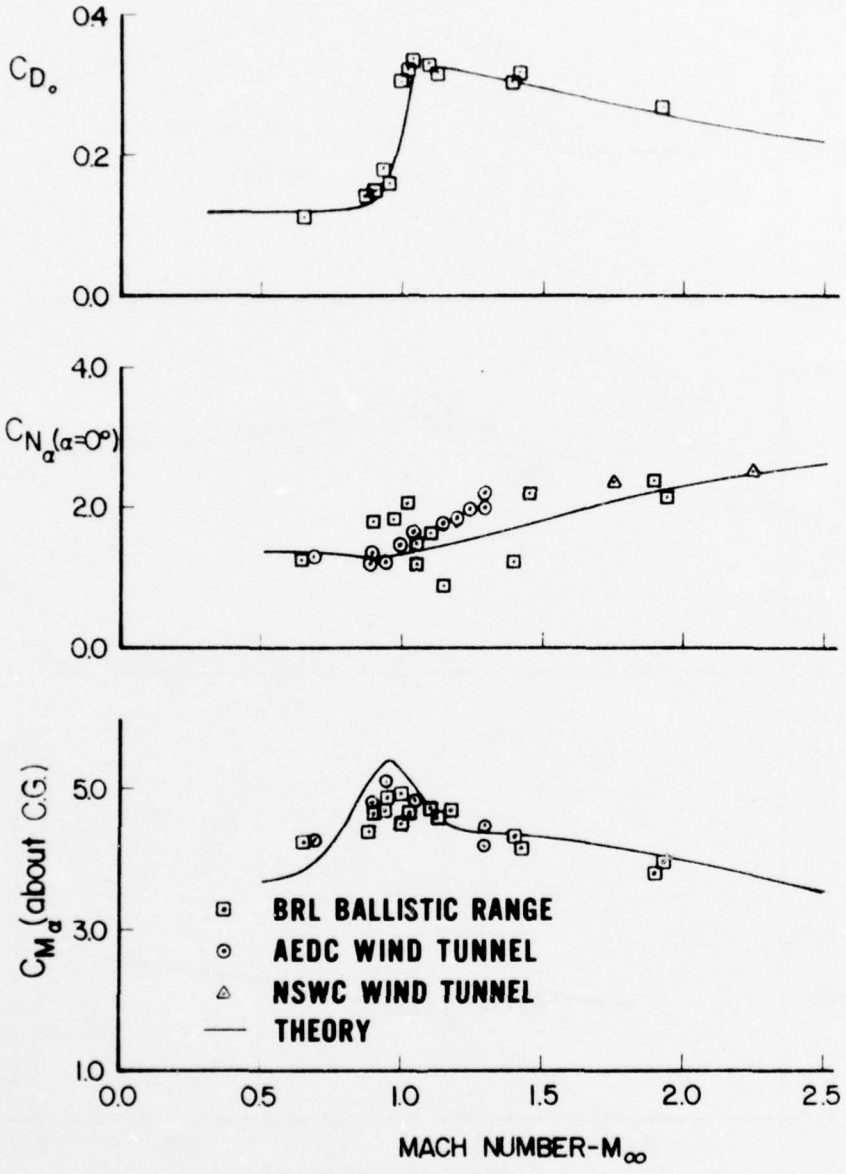

Figure 10. Comparison of Theory and Test Data for Improved 5"/54 Projectile

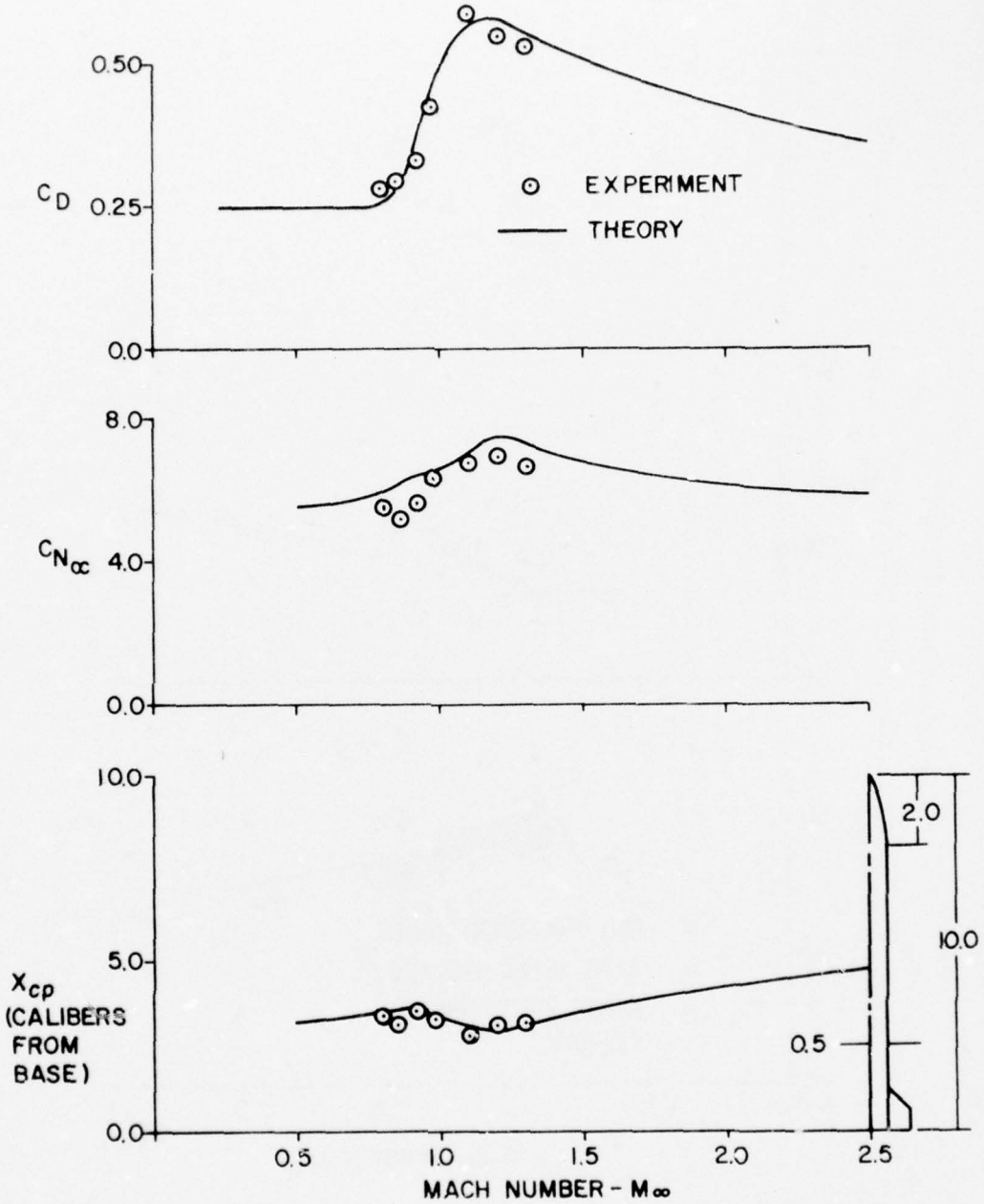

Figure 11. Static Aerodynamics of a Missile Configuration; AR = 1.0, Λ_1 = 53.1°, λ = 0.5, α = 1°

coefficient derivative, and center of pressure with experiment as a function of Mach number and for $\alpha = 1^\circ$. Recall from Figure 3 that for $M_\infty \geq 1.2$, the lift and drag (except for base drag) was calculated numerically, whereas for $0.8 < M_\infty < 1.2$, the theory consists of mostly empirical procedures. For $M_\infty \leq 0.8$, the wing lift is calculated analytically but most other force components are computed empirically. With the exception of the normal force coefficient slope at $M_\infty = 0.8$ and 0.85, the theory is well within 10 percent of experiment. The maximum error in center of pressure for this configuration is 5 percent of the length or half a caliber.

The final example chosen is a complex canard-body-tail configuration. The body nose is 60 percent blunt with two ogive segments and a 0.7 caliber boattail. The canard has an aspect ratio of two with a sweepback angle of 15°. Its shape consists of a sharp wedge leading edge with a constant thickness section following. The trailing edge is truncated parallel to the leading edge. The tail has an aspect ratio of four with cylindrical leading and trailing edges. The tail thickness to chord ratio also varies along the span. The detailed canard and wing geometry listed above is not needed in calculating lift, but it must be known for drag computations. The results of the calculations for this configuration are shown in Figures 12A and 12B. Figure 12A gives the normal force and center of pressure for $M_\infty = 1.6$ and at various angles of attack. Four curves are shown in the figure: canard-body-tail with canards deflected up by 10°, canard-body-tail with no canard deflection, body-tail, and finally, body alone. Several points are worthy of note in this figure. First of all the body alone solution agrees very well with the unpublished experimental data up to $\alpha = 16^\circ$. Above $\alpha = 16^\circ$, the theory is low which is probably due to not taking into account Reynolds number effect in the body crossflow drag coefficient. The next point is that for this configuration, the tail lift is about 10 percent too high and the canard lift about 15 percent too low so that the total lift agrees almost perfectly with the experimental data up to the point where stall begins to occur ($\alpha \geq 14^\circ$). This in turn causes the center of pressure to be up to approximately 0.75 calibers more rearward than the experimental data suggest. It is suspected that the theory being high for the high aspect ratio tail and low for the moderate aspect ratio canard is due to the flowfield interaction effects from the complex configuration and will not, in general, be true for other cases. However, it does indicate that the theory can be used quite effectively in design, even for quite complex wing-body-tail geometries. The final point to be emphasized from Figure 12A is the fact that no attempt has been made to predict stall characteristics. As seen in the figure for this configuration, stall occurs around $\alpha = 15^\circ$ at $M_\infty = 1.6$. However, if the wing thickness or freestream Mach number is changed, the stalling angle of attack will also change.

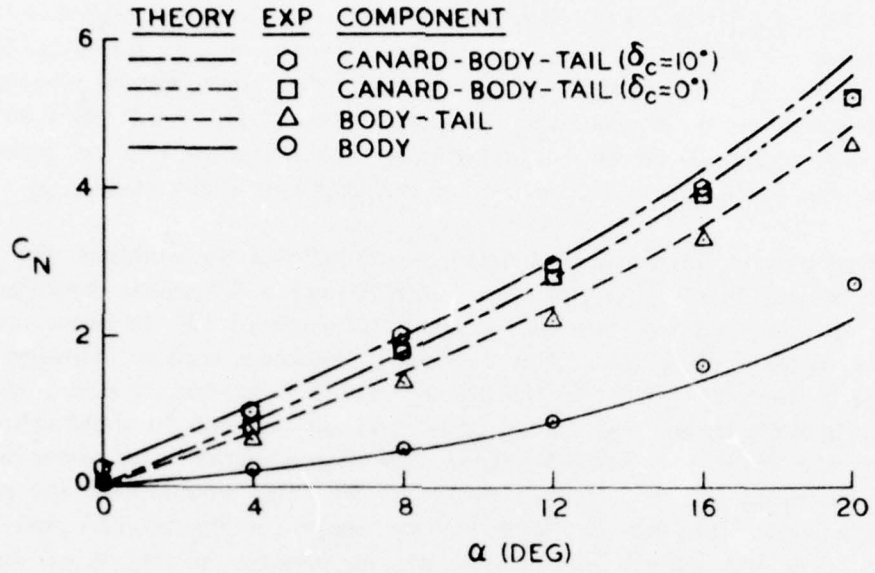

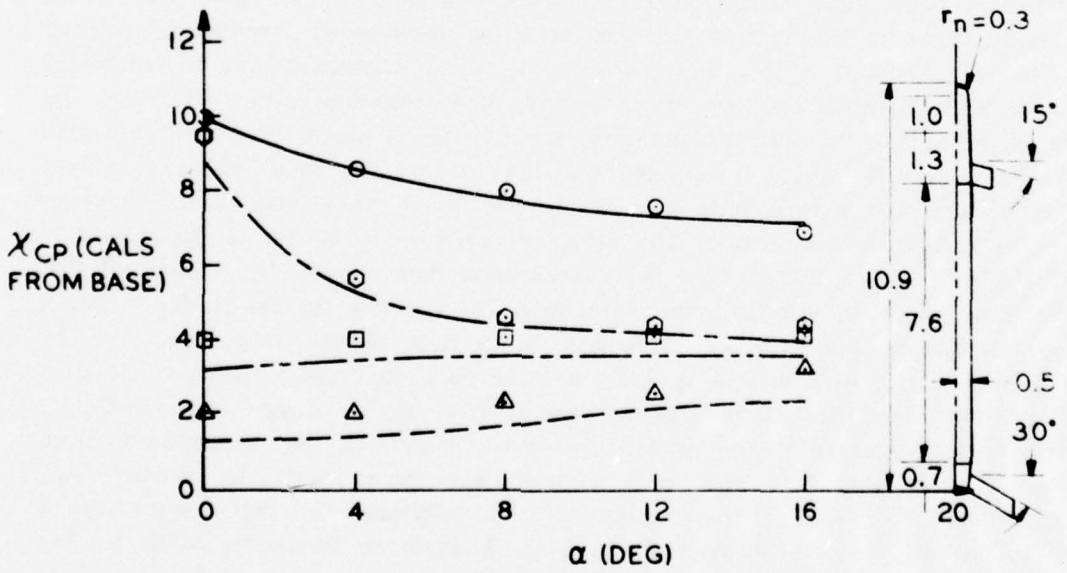

Figure 12A. Normal Forces and Center of Pressure of a Missile Configuration; AR_t = 4, AR_c = 2, M_∞ = 1.6

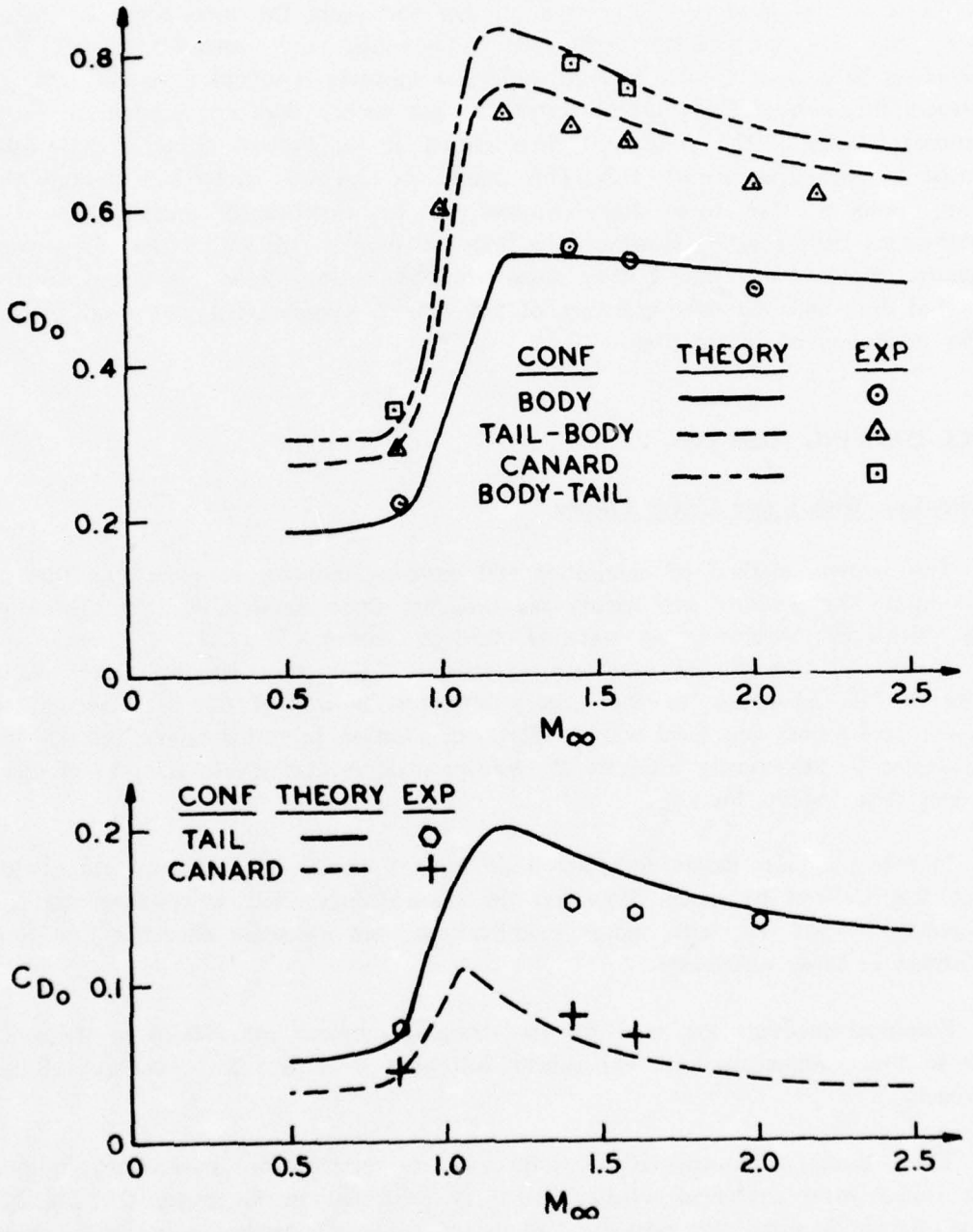

Figure 12B. Drag of a Missile Configuration and Its Components

The drag characteristics for this same missile are shown in Figure 12B. The drag is shown as a function of Mach number and again the total force is broken down into its components: body-alone, body-tail, and canard-body-tail. The body-alone drag is acceptable in supersonic and subsonic flow but is unacceptable in transonic flow where the empirical nature of the theory does not account for nose bluntness correctly. The wing-alone drag shown at the bottom figure, includes the increase in base drag due to tails. This causes the tail drag to be high because the theory predicts this base drag increase to be significantly higher than the experimental data suggest. However, the body-tail drag is still within the ±10-percent category. Finally, the canard drag shown at the bottom figure, is added to the body-tail drag and the overprediction of tail drag is compensated somewhat by the under prediction of canard drag.

ROLL DAMPING MOMENT

Comparison With Exact Linear Theory

The present method of computing roll damping moment in supersonic flow is to compute the pressure coefficients and integrate these numerically over the entire wing planform (assume wing extends through body). This is as opposed to computing C_{ℓ_p} for simple planform geometries using very lengthy closed form solutions. The advantage to the former approach is that if one is interested in pressure coefficients and local wing loadings, in addition to roll damping coefficients, it is easier to numerically integrate the known pressure coefficients than to program the lengthy equations for C_{ℓ_p}.

In subsonic flow, closed form solutions are not possible so no comparisons with exact theories can be made. However, the methodology used is basically that of References 17 and 44, with minor modifications, and extensive checkout has been performed in those references.

Empirical methods are used for the damping moment calculations in transonic flow so that comparison with experiment will have to suffice for check-out of the approach.

Three cases are considered as test cases to compare the numerical solutions with closed form analytical solutions such as presented in References 21 and 22. These include a wing with subsonic leading and supersonic trailing edges and a wing with supersonic leading and trailing edges with the Mach line intersecting the tip

and then the trailing edge. Each of these cases is sufficiently different so as to check the present numerical results with the closed form analytical solutions. These cases are presented in Figures 13, 14, and 15. The results are shown as the local normal force coefficient, c_{N_p}, as a function of the position along the wing semispan. The local normal force coefficient due to a rolling rate p is defined by:

$$c_{N_p} = \frac{1}{b} \int_{x_{LE}}^{x_{TE}} \frac{(\Delta C_p)_p}{pb/2V_\infty} \, dx \tag{53}$$

As expected, the numerical results duplicate the analytical solutions in all cases.

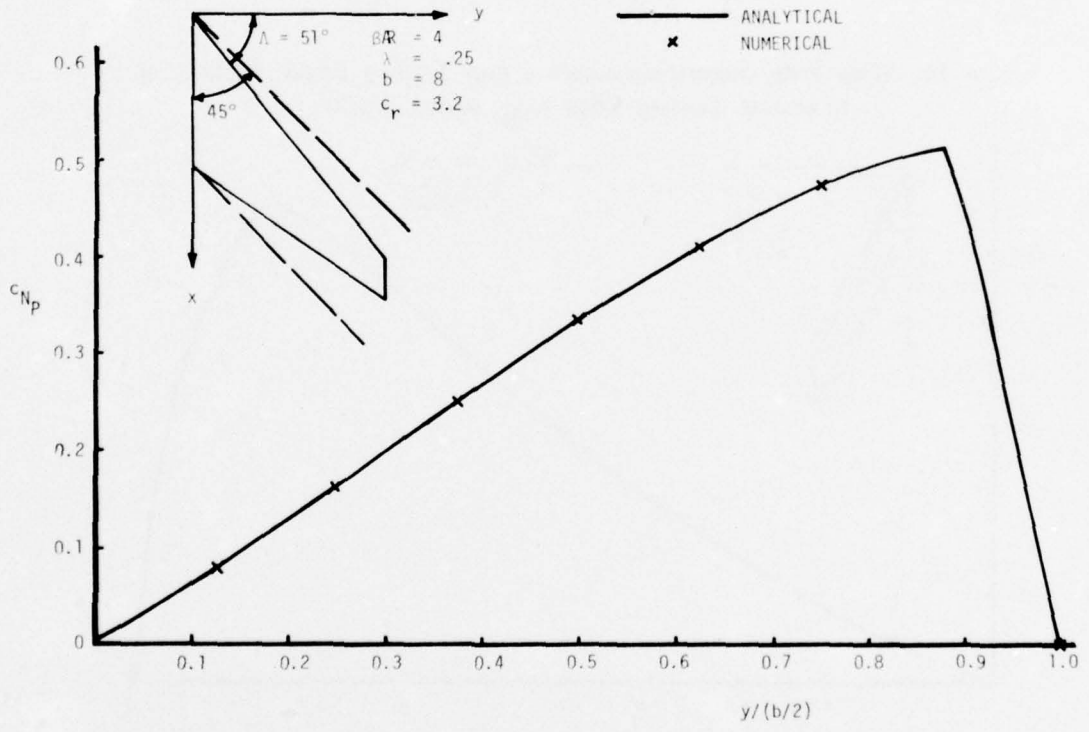

Figure 13. Wing With Subsonic Leading and Supersonic Trailing Edges (c_{N_p} versus y/b/2)

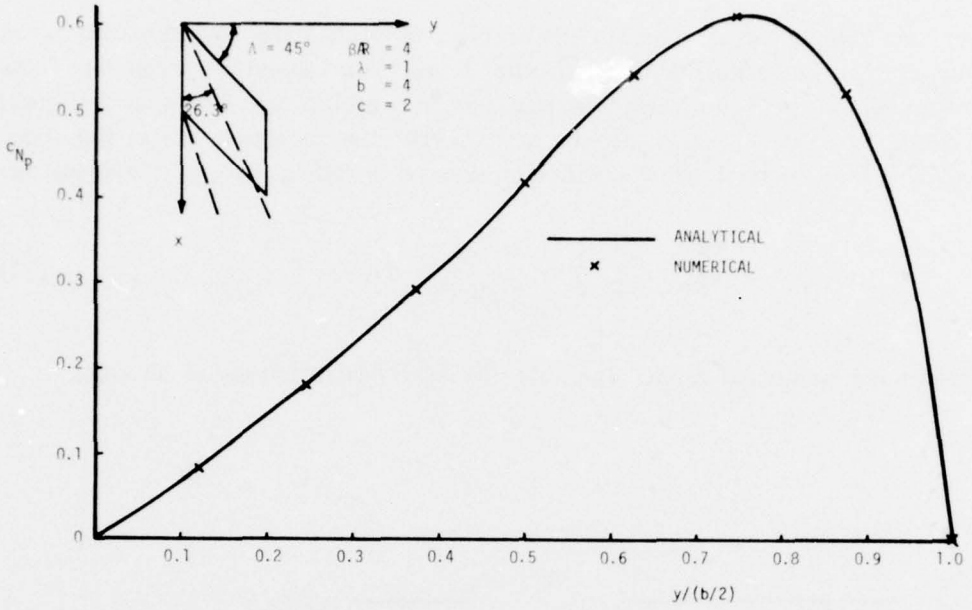

Figure 14. Wing With Supersonic Leading and Trailing Edges; Mach Line Intersects Trailing Edge (c_{N_p} versus y/b/2)

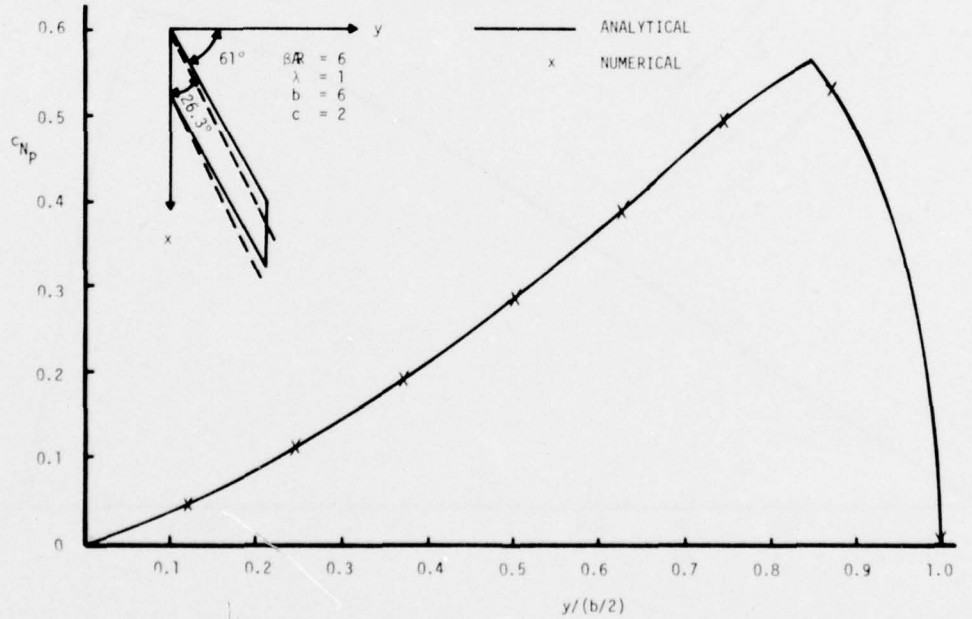

Figure 15. Wing With Supersonic Leading and Trailing Edges; Mach Line Intersects Tip (c_{N_p} versus y/b/2)

Comparison With Experiment

Much work has been done in measuring roll damping, both with rocket powered techniques in the early 1950's and in the last few years with the wind tunnel. Comparison of these experimental results with the 3-D thin wing theory in supersonic flow and lifting surface theory in subsonic flow has, in general, shown reasonable agreement. The theory typically overestimates the actual experimental results on wings where aeroelastic effects are important, particularly in the transonic and low supersonic speed regimes.

Three examples in which roll damping have been calculated are shown in Figures 16, 18, and 19. Figure 16 is a comparison of theory and experiment for the delta wing configuration of Reference 45. As seen in the figure, the present methodology gives reasonable agreement for wing t/c values of 0.04. Apparently, aeroelastic effects were important for this configuration because the linear theory was higher than experiment by as much as 25 percent. This is consistent with the results reported in References 48 and 49 which indicated aeroelastic effects can reduce roll damping by up to 25-30 percent, particularly in transonic flow.

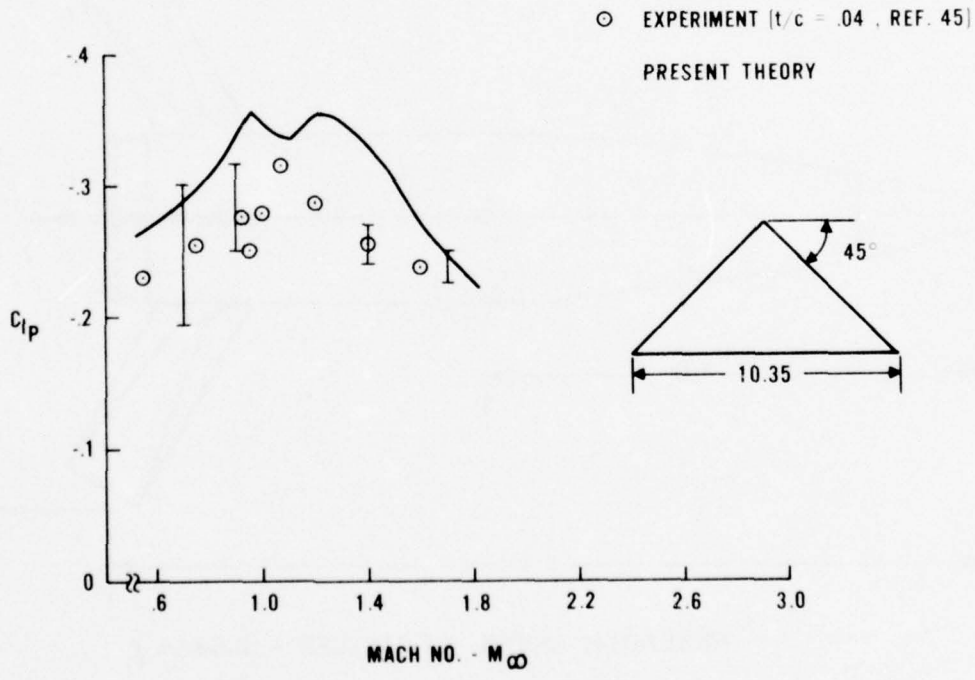

Figure 16. Comparison of Theory and Experiment for Roll Damping of a Delta Wing

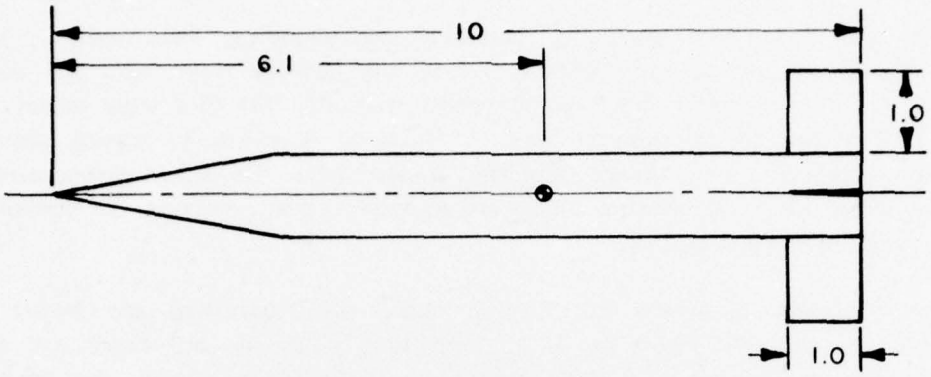

FINNER (1 CALIBER = 3.17cm.)

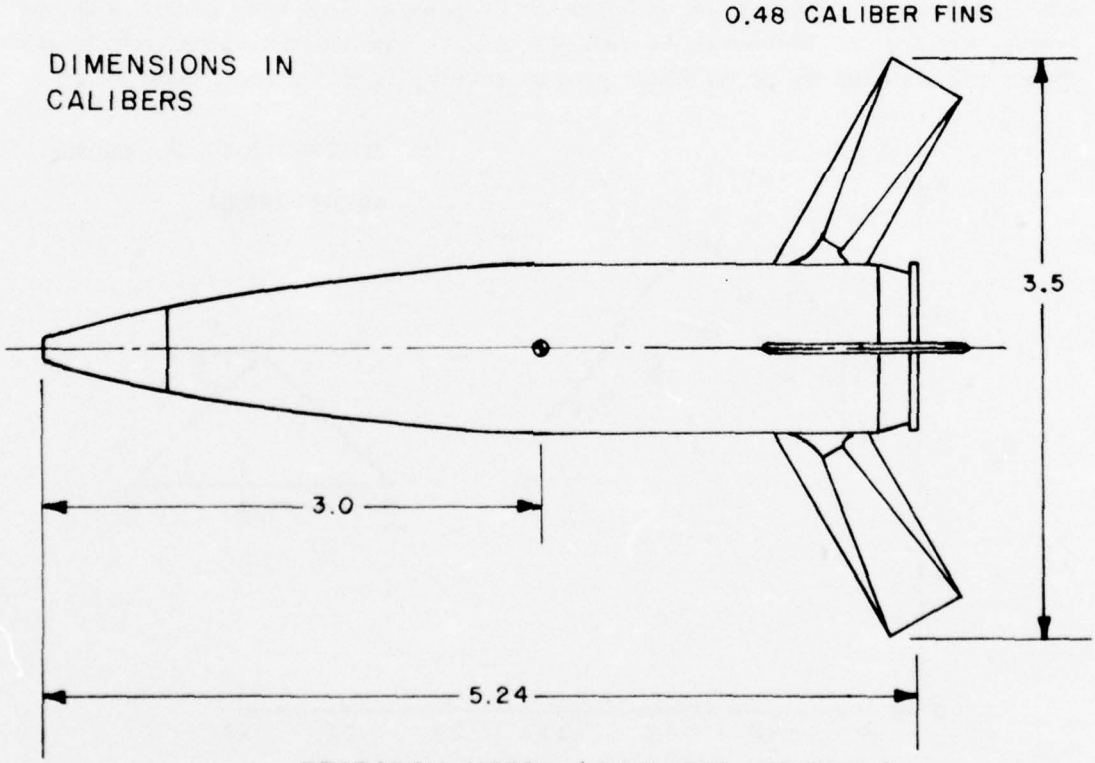

RESEARCH MODEL (1 CALIBER = 12.68cm.)

Figure 17. Body-Tail Configurations

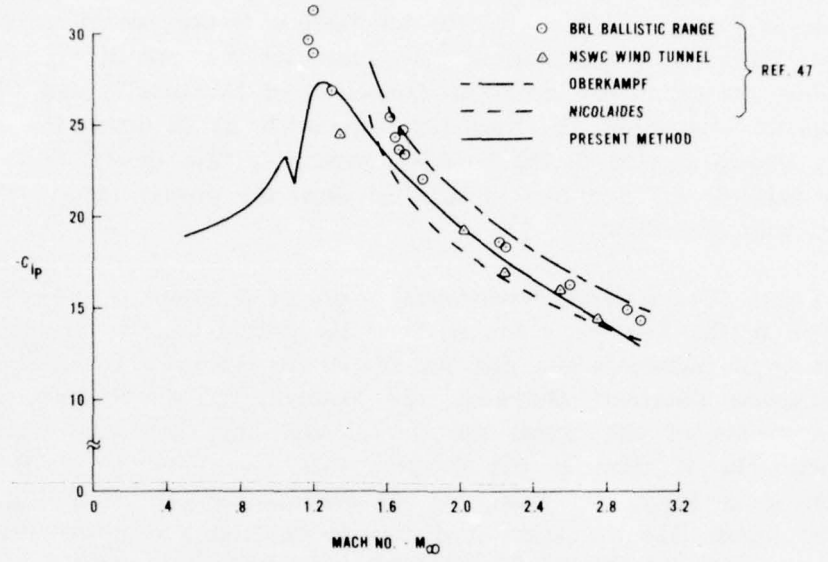

Figure 18. *Roll Damping* Coefficient for Army-Navy Finner

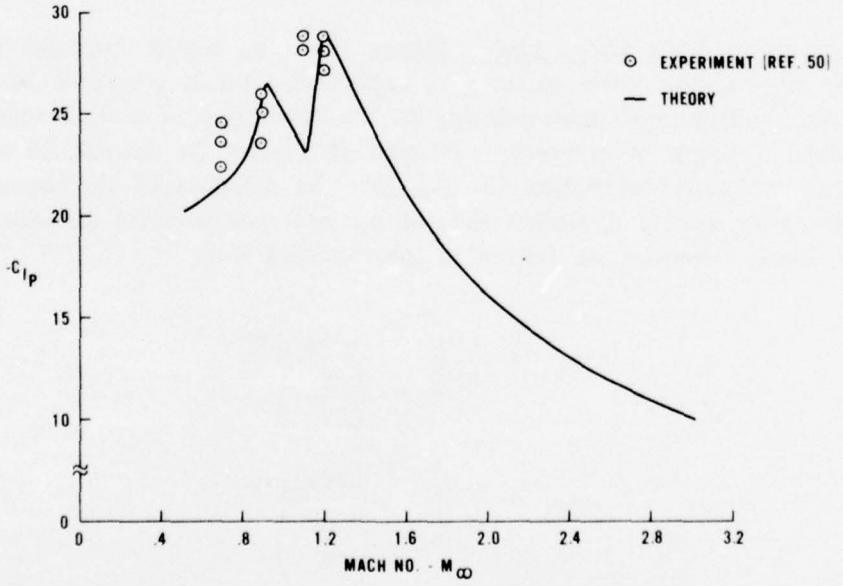

Figure 19. Roll Damping of Navy Research Model Configuration

A second comparison of experiment and the present methodology is shown in Figure 18. This case is for the cruciform wing-body Army-Navy Finner, which is illustrated in Figure 17; therefore, the interference theory procedures can also be employed. Considerable experimental data exists for this case at supersonic speeds. In addition, the quasi-two-dimensional approaches of Nicolaides[48] and Oberkampf[49] are shown for comparison. The theoretical approaches are all within the experimental accuracy, lending support to the linearized supersonic flow theory. Since there were no data available for this case in subsonic flow, the present theory could not be compared with experiment.

In Figure 17 a research development model of a beamrider projectile is shown in addition to the Army-Navy Finner. Since the present analysis for supersonic flow does not handle nonstreamwise tips, the tips of the beamrider are assumed to be in the streamwise direction. Moreover, the assumed tip chords pass through the midchord points of the actual tip chords, and thus the wing surface area is maintained. The variation in roll damping with Mach number is given for this configuration in Figure 19. There are no available damping in roll data for the supersonic region. The theoretical prediction in this region compares favorably with an estimate based upon the experimental lift and center of pressure.

Pitch Damping Moment

Comparison With Exact Linear Theory. For the reason indicated in the roll damping section, the pitch damping in supersonic flow is computed by integrating the pressure distributions corresponding to the two types of motion associated with longitudinal damping. A comparison is made in Figures 20 through 25 between the numerical and analytical results for the spanwise variation of the sectional normal force derivative due to q motion and the sectional normal force derivative due to $\dot{\alpha}$ motion. These quantities are defined in the following way:

$$c_{N_Q} = \frac{1}{c} \int_{x_{LE}}^{x_{TE}} \frac{(\Delta C_p)_q}{\left(\frac{q\bar{c}}{2V_\infty}\right)} dx ,$$

$$c_{N_{\dot{\alpha}}} = \frac{1}{c} \int_{x_{LE}}^{x_{TE}} \frac{(\Delta C_p)_{\dot{\alpha}}}{\left(\frac{\dot{\alpha}\bar{c}}{2V_\infty}\right)} dx .$$

where

$\bar{c}$ is the mean aerodynamic chord.

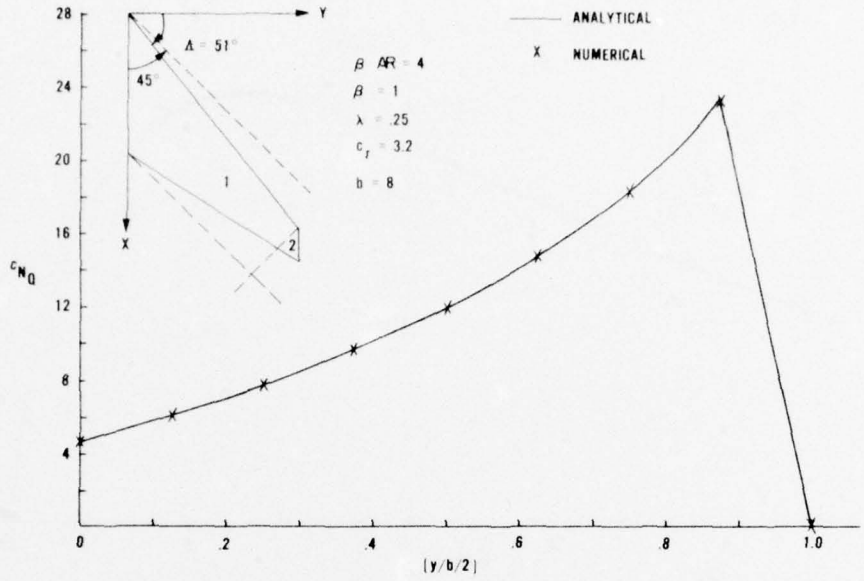

Figure 20. Wing With Subsonic Leading and Supersonic Trailing Edges (c_{N_Q} versus y/b/2)

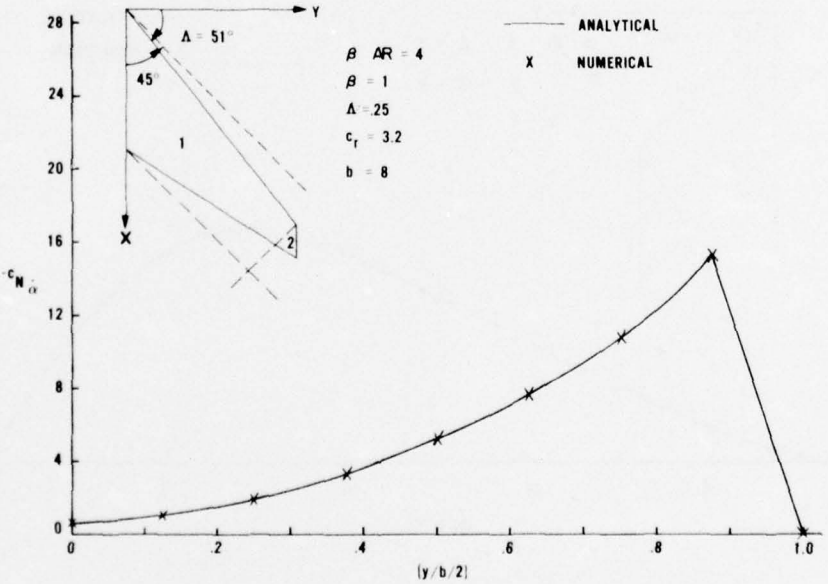

Figure 21. Wing With Subsonic Leading and Supersonic Trailing Edges ($-c_{N_{\dot{\alpha}}}$ versus y/b/2)

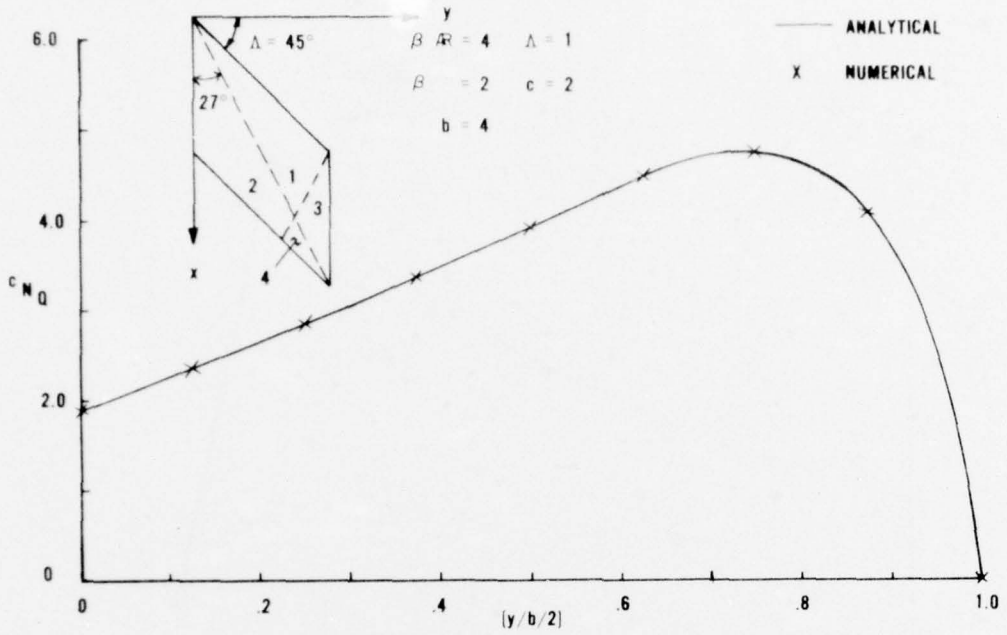

Figure 22. Wing With Supersonic Leading and Trailing Edges; Mach Line Intercepts Trailing Edge (c_{N_Q} versus y/b/2)

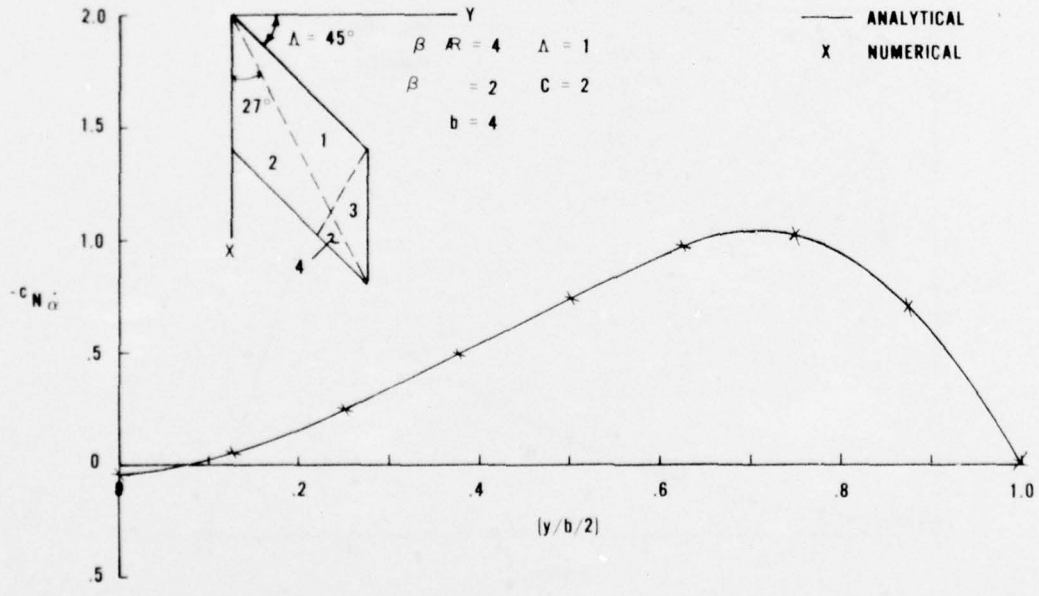

Figure 23. Wing With Supersonic Leading and Trailing Edges; Mach Line Intercepts Trailing Edge ($-c_{N_{\dot{\alpha}}}$ versus y/b/2)

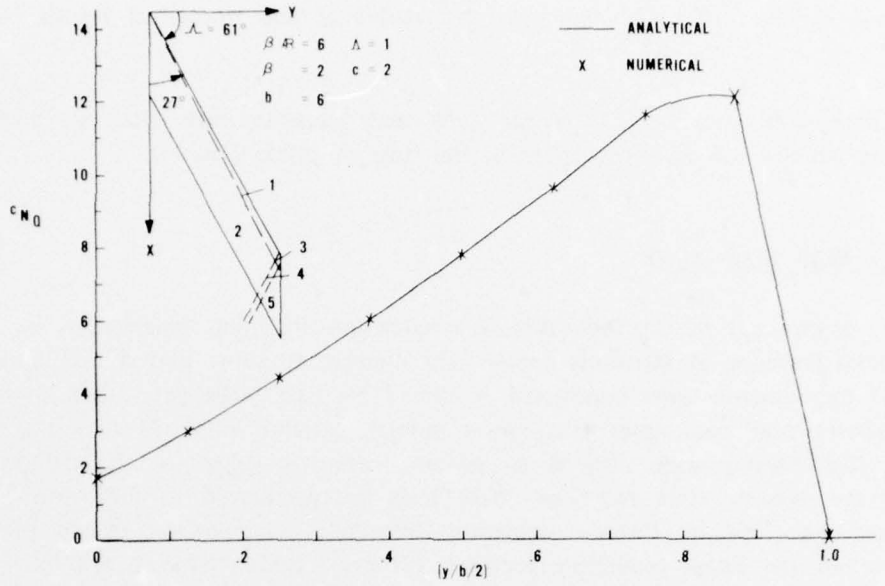

Figure 24. Wing With Supersonic Leading and Trailing Edges; Mach Line Intercepts Tip (c_{N_Q} versus y/b/2)

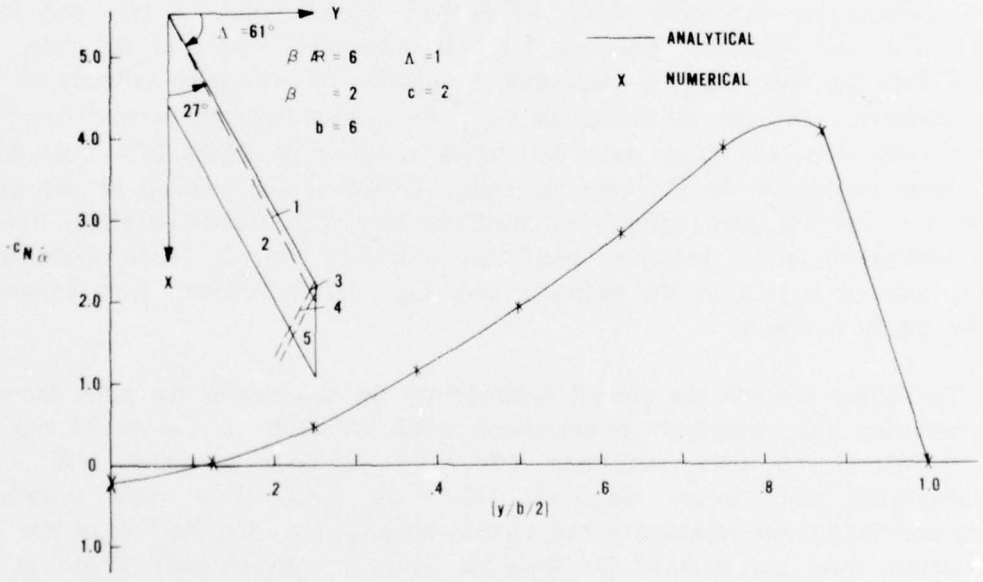

Figure 25. Wing With Supersonic Leading and Trailing Edges; Mach Line Intercepts Tip ($-c_{N_\alpha}$ versus y/b/2)

There are negligible differences between the analytical and numerical results in the figures.

The comments concerning subsonic flow and transonic flow that are made in the previous section are also applicable in the case of pitch damping.

Comparison With Experiment

As a consequence of the reduction in longitudinal damping experienced by most flight vehicles traveling at transonic speeds and undergoing short period oscillations, a number of experiments were conducted in the 1950's to investigate pitch damping. Several experimental techniques (i.e., wind tunnel, ground launched rocket models, full scale flight tests) were utilized to obtain measured values of the damping in pitch. At the present time most of these tests are performed in the wind tunnel using either the free or forced oscillation technique. Comparisons made between these data and the linear prediction methods discussed herein have shown reasonable agreement. That is, trends are generally predicted well, and magnitudes are usually predicted within roughly ±20 percent.

In Figures 26a and 26b the subsonic variation of the quantity $C_{M_Q} + C_{M_{\dot{\alpha}}}$ with Mach number for two delta wings which have aspect ratios of two and four, respectively, are presented. Although there is substantial scatter in the data, the steady damping term C_{M_Q} is considered to provide an acceptable estimate of the total damping. Also, the calculation of C_{M_Q} for a sweptback and tapered wing of aspect ratio three and taper ratio 0.6, which is shown in Figure 27, agrees fairly well with experiment in the subsonic region. However, the peaking of the pitch damping in the transonic region is not predicted very well. This is essentially due to the application of an empirical calculation procedure that is based upon linear theory and the neglect of the unsteady term $C_{M_{\dot{\alpha}}}$, which becomes more important in the transonic region.

To further evaluate the present methodology for determining the pitch damping the following three wing-body combinations, which are shown in Figures 28 and 29, are considered: (1) delta wing-body (AR = 2), (2) delta wing-body (AR = 4), (3) sweptback and tapered wing-body (AR = 3). Since these three wing-body configurations do not represent actual tactical weapons (i.e., the location of the axis of rotation from the nose of the body in terms of percent body length is too high), the body contribution to the total pitch damping is a theoretical estimate rather than the usual empirical one. Test data for $C_{M_Q} + C_{M_{\dot{\alpha}}}$ as a function of Mach number and the corresponding theoretical predictions are presented for these

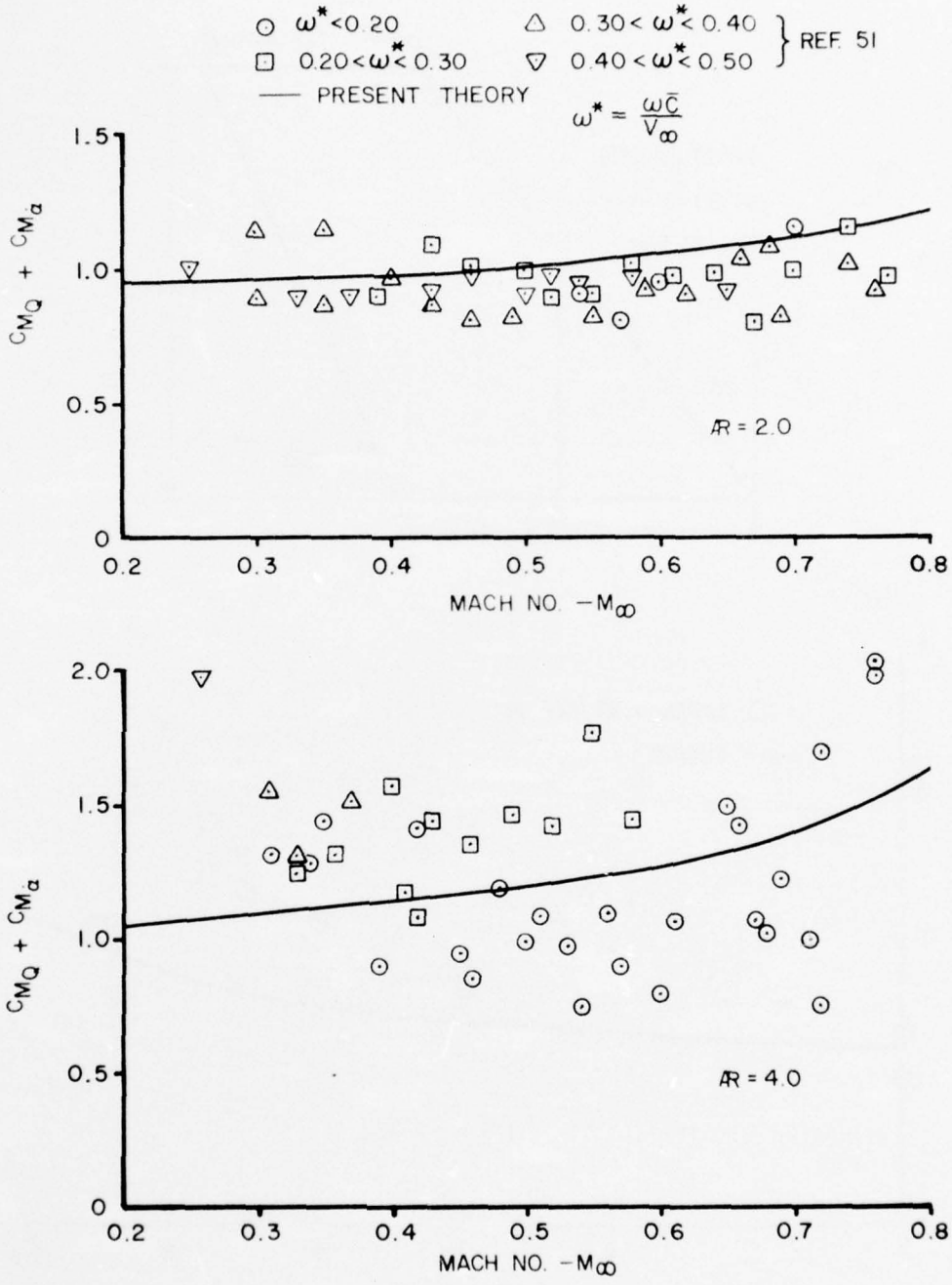

Figure 26. Pitch Damping of Two Delta Wings Oscillating About Axis Through $c_R/2$

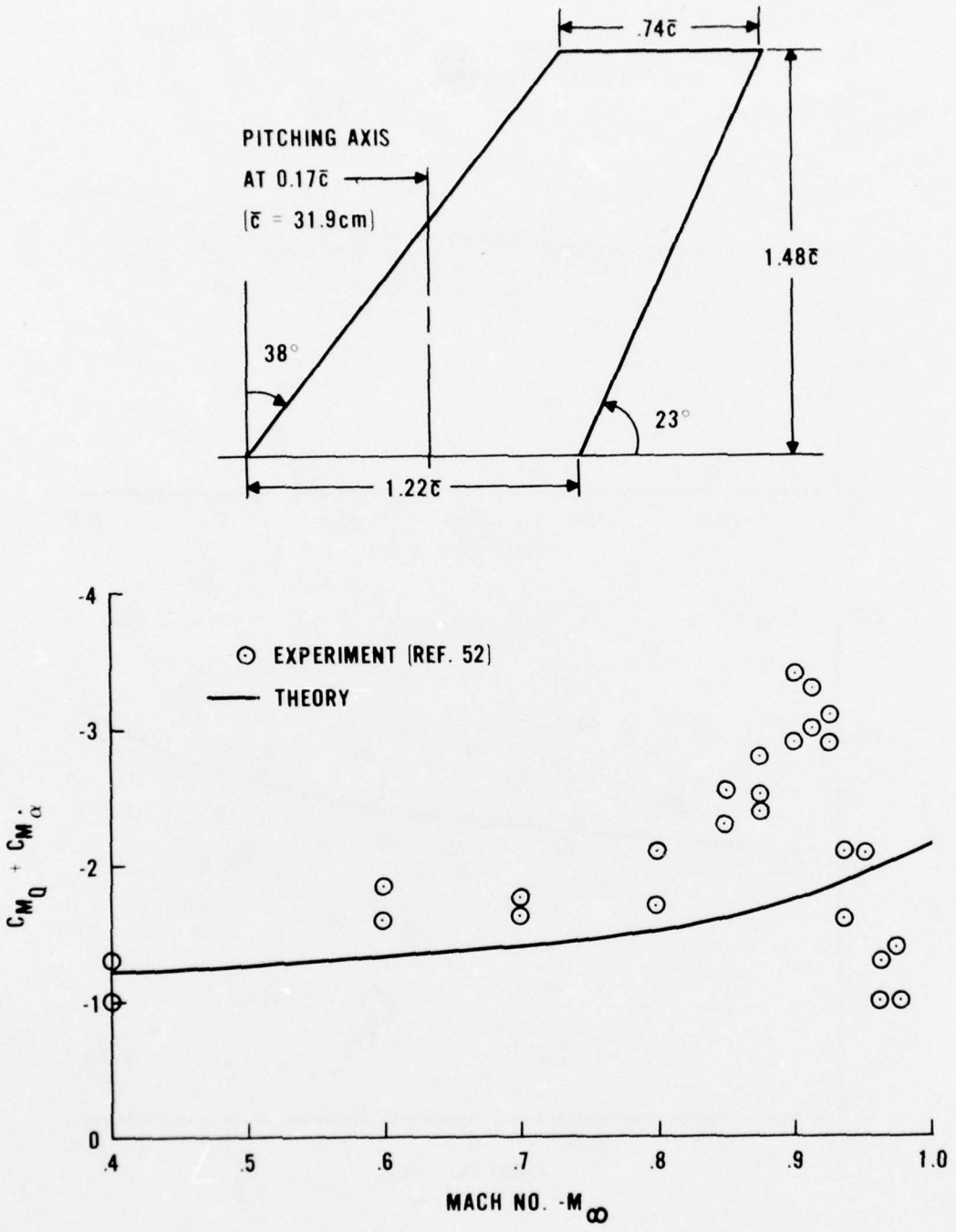

Figure 27. Pitch Damping of a Sweptback and Tapered Wing (AR = 3)

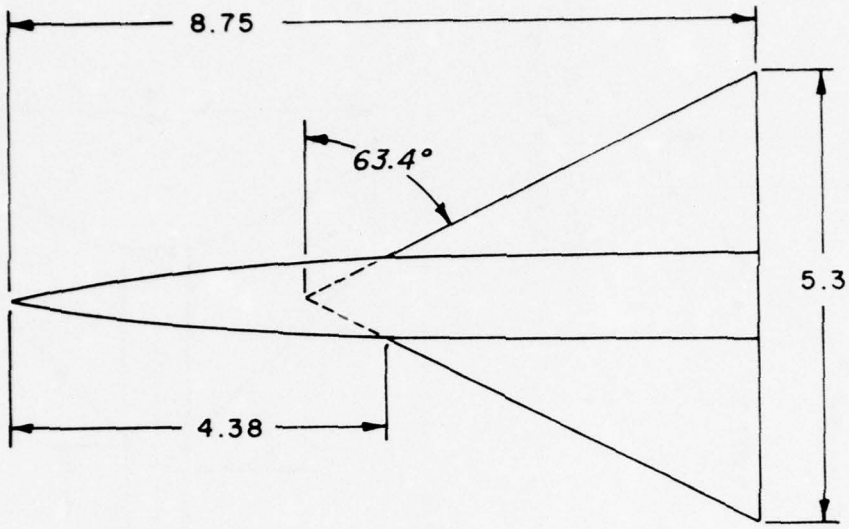

DIMENSIONS IN CALIBERS
1 CALIBER = 10.16cm.

Figure 28. Delta Wing-Body (AR = 2)

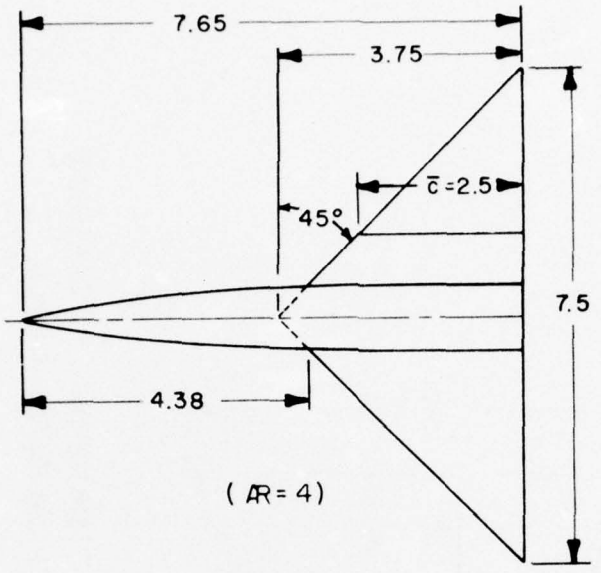

DIMENSIONS IN CALIBERS
1 CALIBER = 10.16cm

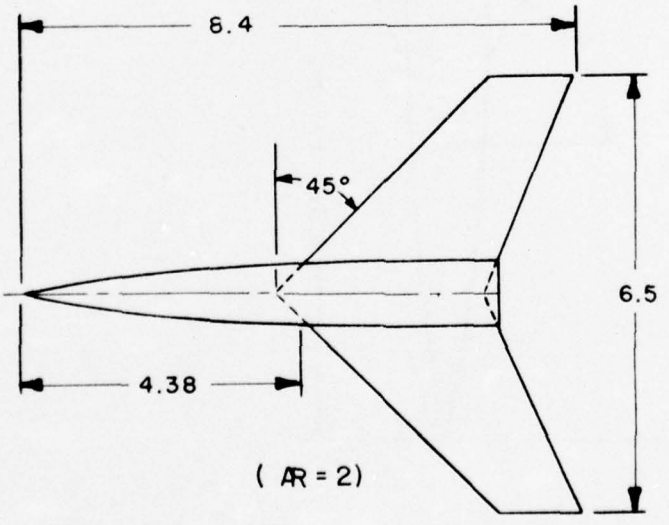

Figure 29. Delta Wing-Body and Sweptback and Tapered Wing-Body

three configurations in Figures 30 through 32. For all three cases the agreement between theory and experiment is fairly good in the supersonic speed regime. The subsonic prediction is reasonable in all cases since the maximum deviation is about 22 percent. In case (1) the transonic peak is underestimated, and the predicted force break Mach number is higher than that depicted by the data (i.e., theory gives peak at M = 1.14 while experiment gives peak at M = .98). As mentioned previously, this is a result of the empirical nature of the transonic scheme and the assumption that $C_{M_{\dot{\alpha}}}$ is approximately zero. Configurations (2) and (3) encounter a region of instability in the transonic region. The method used here to obtain pitch damping indicates if a configuration is stable or unstable, which is sufficient with respect to current stated objectives, but it does not predict the magnitude of the instability.

Finally, the pitch damping of the Army-Navy Finner and a research development model of a beamrider projectile are examined. Since there are no longitudinal damping data available through the total flight range for a given center of gravity location in the case of the basic Finner, theory and experiment are compared for two different center of gravity locations, i.e., x_{CG} = 6.1 calibers and x_{CG} = 6.92 calibers. Good agreement is exhibited in Figure 33a for the supersonic regime. In Figure 33b the rapid decrease in the damping at transonic speeds is not predicted. In the case of the beamrider the pitch damping is given in Figure 34. There is a maximum deviation of 23 percent between experimental data and theory. The decrease in the theoretical $C_{M_Q} + C_{M_{\dot{\alpha}}}$ in the lower supersonic Mach number range is due to the extension of the wing through the body in the interference computational procedure. That is, there is a reduction in wing tip effects because the intersection of the tips by the Mach lines emanating from the apex of the total wing are downstream of the intersections by the Mach lines originating from the apexes of the exposed wing panels. The maximum reduction in total damping, which occurs at M = 1.2, is approximately 6 percent.

COMPUTER PROGRAM

A computer program, which utilizes the theory discussed in this report and References (6) and (7), has been developed to calculate both the static and dynamic aerodynamics for tactical weapons to Mach number 3 and angle of attack of 15°. The primary inputs required by this program to determine the aerodynamics of a given flight configuration are geometrical ones, i.e., body length, variation in body shape, wing planform shape in terms of physical dimensions, etc. Important features of this program are its fast execution time and low cost. For example, it takes

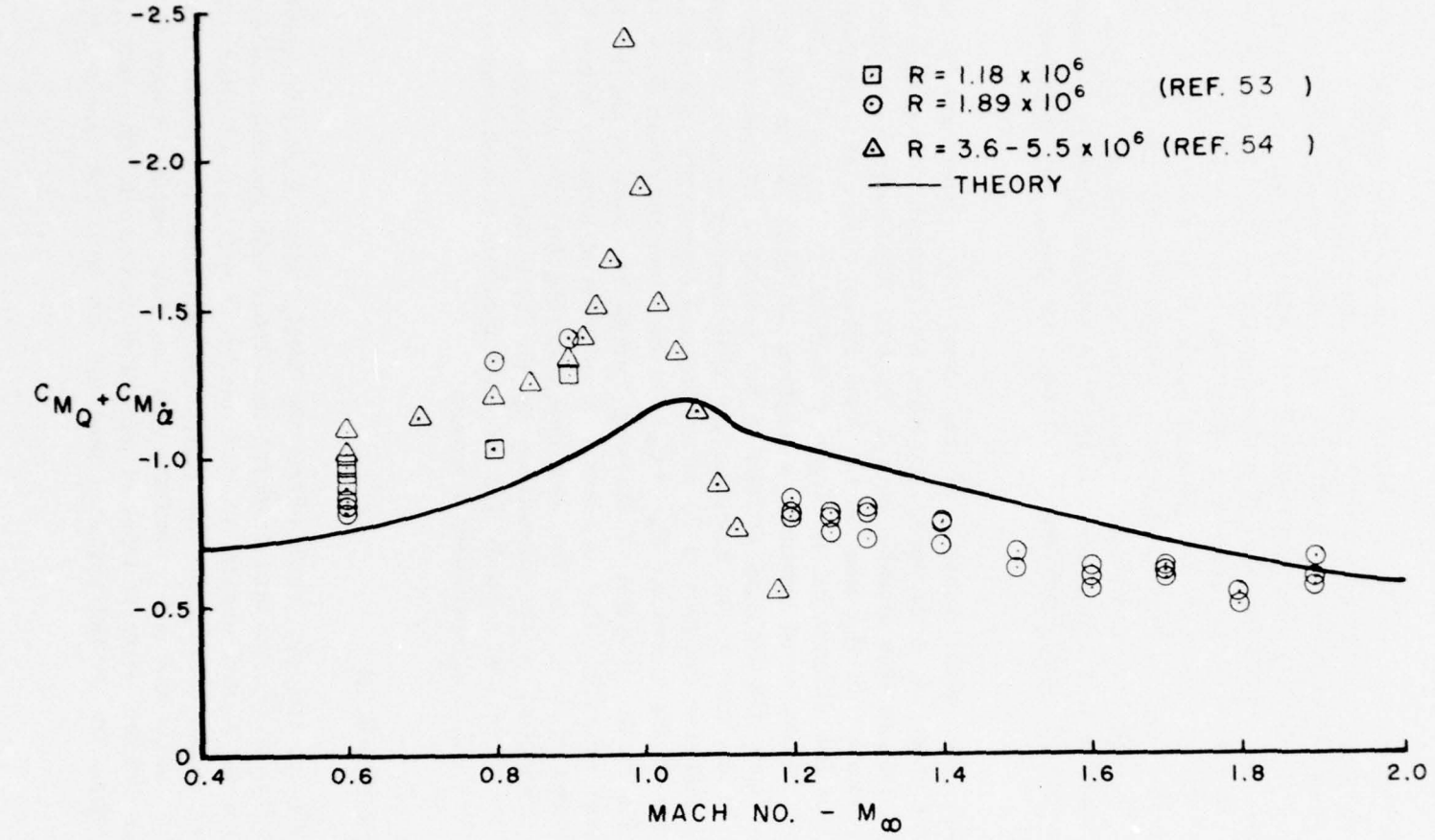

Figure 30. Pitch Damping of Delta Wing-Body (AR = 2)

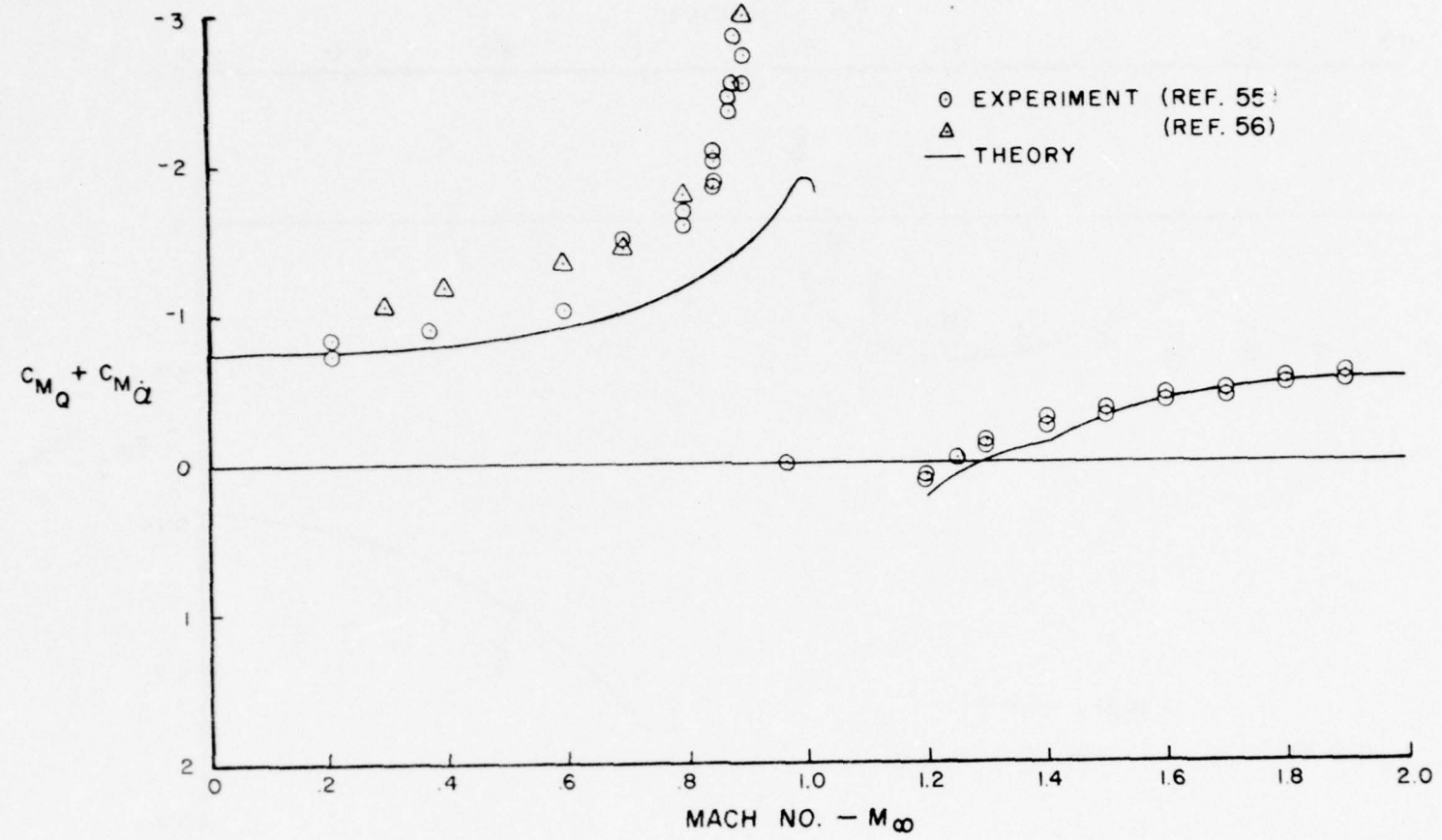

Figure 31. Pitch Damping of Delta Wing-Body (AR = 4)

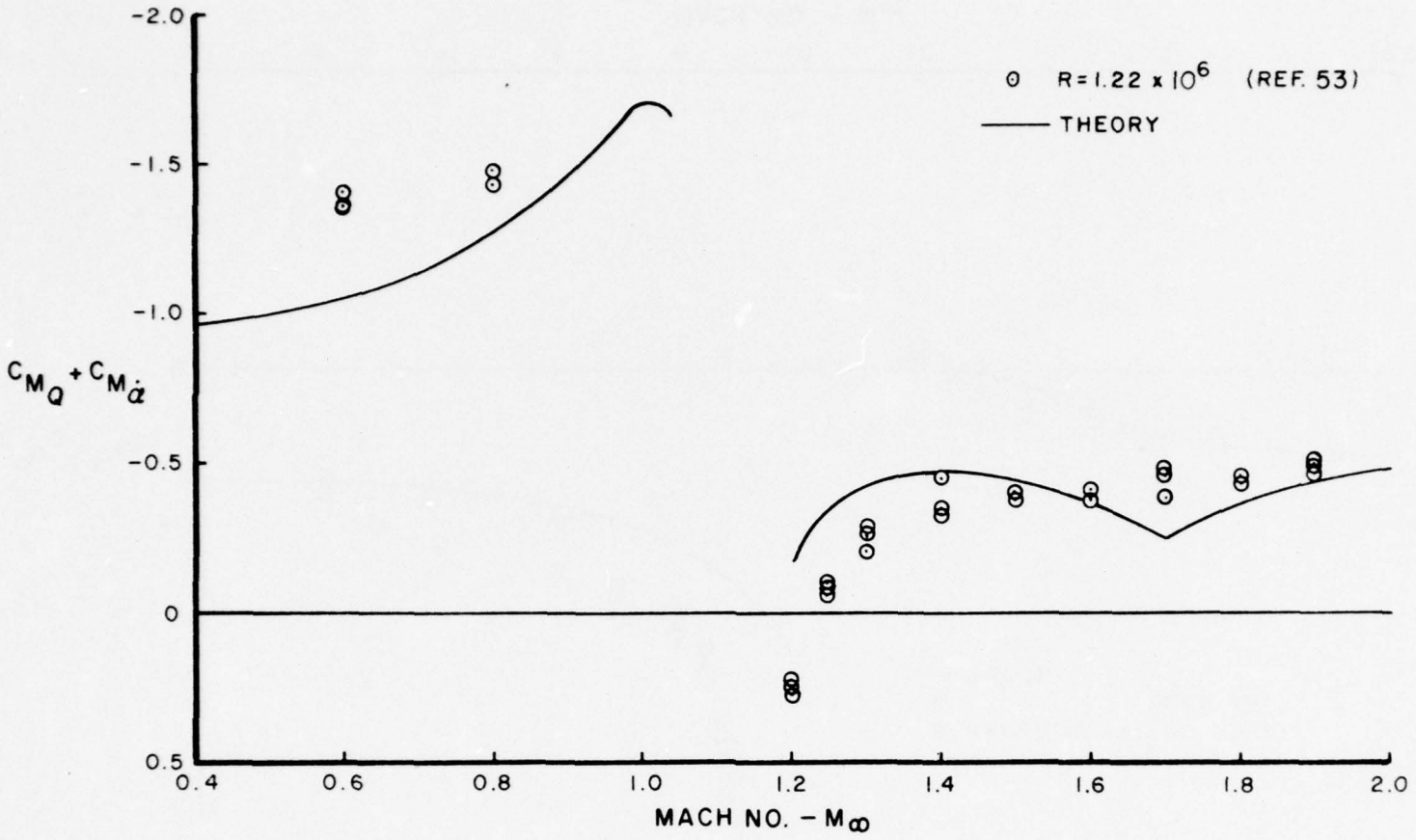

Figure 32. Pitch Damping of Sweptback and Tapered Wing-Body (AR = 3)

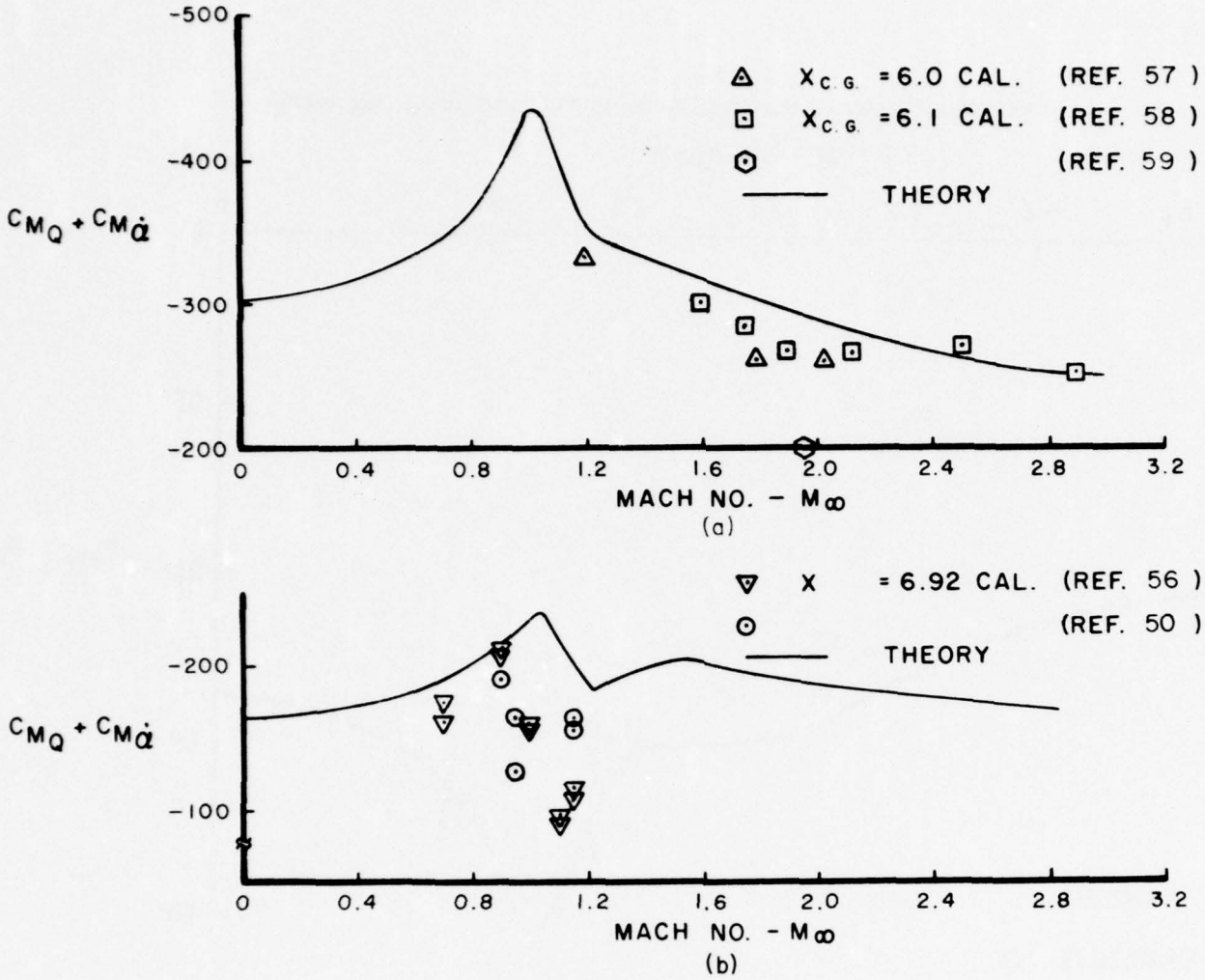

Figure 33. Pitch Damping of Army-Navy Finner

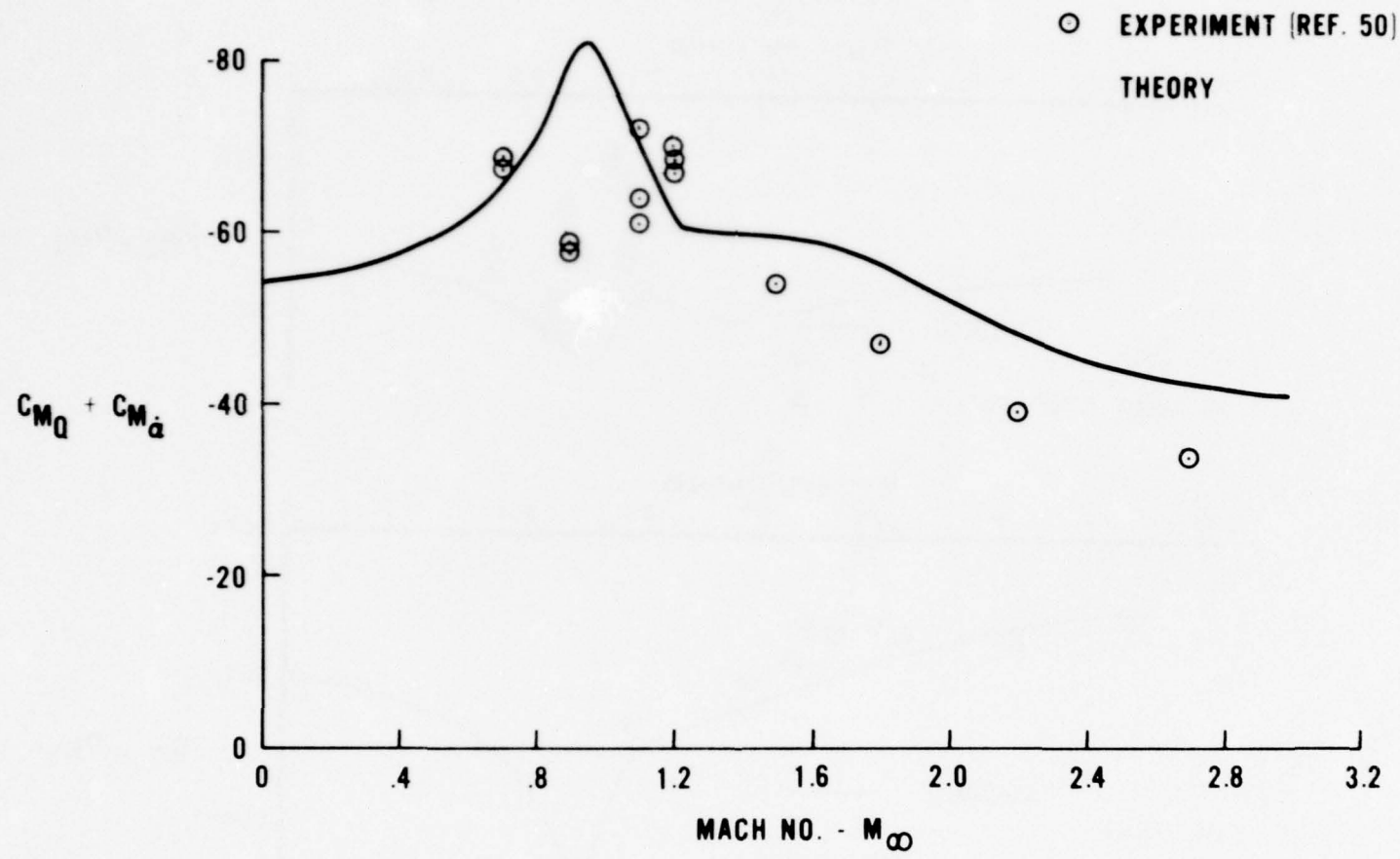

Figure 34. Pitch Damping of Navy Research Model Configuration

about 5 min on the CDC 6700 machine at a cost of about $50 to determine the aerodynamic coefficients at 10 Mach numbers for a configuration such as the beamrider. A detailed description of the computer program, along with several example cases and a Fortran listing of the program, are given in Part II of the present report.

CONCLUSIONS AND RECOMMENDATIONS

1. A general method has been developed consisting of several theoretical and empirical procedures to calculate lift, drag, pitching moment, magnus moment, roll damping moment and pitch damping moment on wing-body-tail configurations from Mach number zero to three and angles of attack up to stall.

2. Comparison of the overall methodology with experiment for several configurations indicates that accuracies of ±10 percent can be obtained for static force coefficients of most configurations. Dynamic force and moment coefficients are within 25 percent of experimental data for most cases. This is at a cost of less than $10 per Mach number for the entire set of aerodynamic coefficients.

3. If roll damping is desired within ±10 percent for most configurations, thickness and aeroelastic effects should be accounted for.

4. There is still no good method to compute magnus forces and moments on typical ordnance.

5. The prediction methodology in transonic flow is almost entirely empirical due to the current state-of-the-art in simple (but yet accurate) analytical methods for use in flow computations. It is thus recommended that work be continued in this Mach number regime with reasonable emphasis on simple techniques.

6. Due to increasing performance requirements for tactical weapons, it now appears appropriate to extend the present design methodology to incorporate higher Mach number, higher angle of attack, and airbreathing configurations.

REFERENCES

1. Douglas Aircraft Co., Inc., **USAF Stability and Control DATCOM**, Revisions by Wright-Patterson Air Force Base, July 1963, 2 Vols.

2. F. A. Woodward,, ***Analysis and Design of Wing-Body Combinations at Subsonic and Supersonic Speeds***, Journal of Aircraft, Vol. 5, No. 6, 1968, pp. 528-534.

3. B. F. Saffell, Jr., M. L. Howard, and E. N. Brooks, Jr., ***A Method for Predicting the Static Aerodynamic Characteristics of Typical Missile Configurations for Angles-of-Attack to 180 Degrees***, NSRDC Report 3645, 1971.

4. R. H. Whyte, ***Spinner – A Computer Program for Predicting the Aerodynamic Coefficients of Spin Stabilized Projectiles***, General Electric Class 2 Reports, 1969.

5. F. G. Moore, ***Aerodynamic Drag and Lift of General Body Shapes at Subsonic, Transonic, and Supersonic Mach Numbers***, AGARD Conference preprint No. 124 on Aerodynamic Drag, Paper No. 2, 1973.

6. F. G. Moore, ***Body Alone Aerodynamics of Guided and Unguided Projectiles at Subsonic, Transonic, and Supersonic Mach Numbers***, NWL TR-2796, 1972.

7. F. G. Moore, ***Aerodynamics of Guided and Unguided Weapons: Part I – Theory and Application***, NWL TR-3018, December 1973.

8. F. G. Moore and C. W. McKerley, ***Aerodynamics of Guided and Unguided Weapons; Part II – Computer Program and Usage***, NWL TR-3036, 1974.

9. F. G. Moore, ***Static Aerodynamics of Missile Configurations for Mach Number Zero to Three***, AIAA Paper No. 74-538.

10. M. D. Van Dyke, ***First and Second-Order Theory of Supersonic Flow Past Bodies of Revolution***, JAS, Vol. 18, No. 3, March 1951, pp. 161-179.

11. H. S. Tsien, ***Supersonic Flow Over an Inclined Body of Revolution***, JAS, Vol. 5, No. 12, October 1938, pp. 480-483.

12. J. M. Wu and K. Aoyoma, ***Transonic Flow-Field Calculation Around Ogive Cylinders by Nonlinear-Linear Stretching Method***, U. S. Army Missile Command

Technical Report No. RD-TR-70-12, April 1970. Also AIAA 8th Aerospace Sciences Meeting, AIAA Paper 70-189, January 1970.

13. E. R. Van Driest, ***Turbulent Boundary Layer in Compressible Fluids***, JAS, Vol. 18, No. 3, pp. 145-160, 216.

14. J. H. Allen and E. W. Perkins, ***Characteristics of Flow Over Inclinded Bodies of Revolution***, NACA RM A 50L07, 1965.

15. E. S. Love, ***Base Pressure at Supersonic Speeds on Two-Dimensional Airfoils and on Bodies of Revolution With and Without Turbulent Boundary Layers***, NACA TN-3819, 1957.

16. H. Ashley and M. Landahl, ***Aerodynamics of Wings and Bodies***, Addison-Wesley Publishing Company, Reading, Massachusetts.

17. W. R. Chadwick, ***The Application of Non-Planar Lifting Surface Theory to the Calculation of External Store Loads***, Complete 1972.

18. R. T. Jones and Doris Cohen, ***High Speed Wing Theory***, Princeton Aeronautical Paperbacks, Number 6, 1960.

19. D. R. Chapman, W. R. Wimbrow, and R. H. Kester, ***Experimental Investigation of Base Pressure on Blunt-Trailing-Edge Wings at Supersonic Velocities***, NACA Rep. 1109, 1952 (supersedes NACA TN-2611).

20. W. C. Pitts, J. N. Nielsen, and G. E. Kaattari, ***Lift and Center of Pressure of Wing-Body-Tail Combinations at Subsonic, Transonic, and Supersonic Speeds***, NACA TR 1307, 1957.

21. J. C. Martin and I. Jeffreys, ***Span Load Distribution Resulting From Angle-of-Attack, Rolling, and Pitching for Tapered Sweptback Wings With Streamwise Tips***, NACA TN 2643, 1952.

22. F. S. Malvestuto, Jr., K. Margolis, and H. Ribner, ***Theoretical Lift and Damping in Roll at Supersonic Speeds of Thin Sweptback Tapered Wings With Streamwise Tips, Subsonic Leading Edges, and Supersonic Trailing Edges***, NACA TR 970, 1950.

23. V. E. Lockwood, *Effects of Sweep on the Damping-in-Roll Characteristics of Three Sweptback Wings Having an Aspect Ratio of 4 at Transonic Speeds*, NACA RM L50J19, December 1950.

24. J. L. Edmondson, *Damping in Roll of Rectangular Wings of Several Aspect Ratios and NACA 65A Series Airfoil Sections of Several Thicknesses Ratios at Transonic and Supersonic Speeds as Determined With Rocket-Powered Models*, NACA RM L50E26, 1950.

25. G. J. Adams and D. W. Dugan, *Theoretical Damping in Roll and Rolling Moment Due to Differential Wing Incidence for Slender Cruciform Wings and Wing-Body Combinations*, NACA TR 1088, 1952.

26. A. Kuethe and J. Schetzer, *Foundations of Aerodynamics*, John Wiley & Sons, New York, 1960.

27. J. N. Nielsen, **Missile Aerodynamics**, the McGraw-Hill Book Company, Inc., New York, 1960.

28. H. R. Kelly and R. G. Thacker, *The Effect of High Spin on the Magnus Force on a Cylinder at Small Angles of Attack*, NAVORD Report 5036, February 1956.

29. J. C. Martin, *On Magnus Effects Caused by the Boundary Layer Displacement Thickness on Bodies of Revolution at Small Angles of Attack*, Ballistic Research Laboratories Report No. 870, June 1955.

30. R. Sedney, *Laminar Boundary Layer on a Spinning Cone at Small Angles of Attack*, Ballistic Research Laboratories Report No. 991, September 1956.

31. H. R. Vaughn and G. E. Reis, *A Magnus Theory for Bodies of Revolution*, SC-RR-720537, January 1973.

32. G. Y. Graff and F. G. Moore, *Effects of Boattail Shapes on Magnus*, NSWC TR-3581, January 1977.

33. A. E. Bryson, *Stability Derivations for a Slender Missile With Application to a Wing-Body-Vertical Tail Configuration*, JAS, Vol. 20, No. 5, 1953.

34. W. P. Rodden, J. P. Giesing, and Kálmán, *New Developments and Applications of the Subsonic Doublet-Lattice Method for Nonplanar Configurations*, AGARD Paper No. 4 (Douglas Paper 5826), November 1970.

35. J. C. Houbolt, *Some New Concepts in Oscillatory Lifting Surface Theory*, AFFDL-TR-69-2, June 1969.

36. E. V. Laitone and E. R. Walters, ***The Application of Non-Stationary Airfoil Theory to Dynamic Stability Derivatives***, JAS, March 1951.

37. M. Goland, ***The Quasi-Steady Air Forces for Use in Low-Frequency Stability Calculations***, JAS, Vol. 17, No. 10, October 1950.

38. M. Tobak and H. C. Lessing, ***Estimation of Rotary Stability Derivatives at Subsonic and Transonic Speeds***, NATO Report 343, April 1961.

39. I. J. Cole and K. Margolis, ***Lift and Pitching Moment at Supersonic Speeds Due to Constant Vertical Acceleration for Thin Sweptback Tapered Wings With Streamwise Tips, Supersonic Leading and Trailing Edges***, NACA TN 3196, July 1954.

40. J. C. Martin, K. Margolis, and I. Jeffreys, ***Calculation of Lift and Pitching Moments Due to Angle of Attack and Steady Pitching Velocity at Supersonic Speeds for Thin Sweptback Tapered Wings With Streamwise Tips and Supersonic Leading and Trailing Edges***, NACA TN 2699, June 1952.

41. F. S. Malvestuto and D. M. Hoover, ***Lift and Pitching Derivatives of Thin Sweptback Tapered Wings With Streamwise Tips and Subsonic Leading Edges at Supersonic Speeds***, NACA TN 2294, February 1951.

42. J. C. Evvard, ***Use of Source Distributions for Evaluating Theoretical Aerodynamics of Thin Finite Wings at Supersonic Speeds***, NACA Rep. 951.

43. J. C. Craft and J. Skorupski, ***Static Aerodynamic Stability Characteristics of Munitions Designs at Transonic Mach Numbers***, U. S. Army Missile Command, Redstone Arsenal, Alabama, 1973.

44. J. W. Purvis, ***Lifting Surface Theory Calculations of Aerodynamic Wing-Tail Load Distributions During Subsonic Maneuvers***, NWL-2787, 1972.

45. W. M. Bland, Jr. and C. A. Sandahl, ***A Technique Utilizing Rocket-Propelled Test Vehicles for the Measurement of the Damping in Roll of Sting-Mounted Models and Some Initial Results for Delta and Unswept Tapered Wings***, NACA TN 3314, 1955.

46. E. C. Sanders, Jr. and J. L. Edmondson, ***Damping in Roll of Rocket-Powered Test Vehicles Having Swept, Tapered Wings of Low Aspect Ratio***, NACA RM L51G06, October 1951.

47. J. L. Edmondson and E. C. Sanders, Jr., ***A Free-Flight Technique for Measuring Damping in Roll by Use of Rocket-Powered Models and Some Initial Results for Rectangular Wings***, NACA RM L9I01, 1949.

48. R. E. Bolz and J. D. Nicolaides, ***A Method of Determining Some Aerodynamic Coefficients from Supersonic Free-Flight Tests of a Rolling Missile***, Journal of the Aeronautical Sciences, Vol. 17, No. 10, October 1950, pp. 609-621.

49. W. L. Oberkampf, ***Theoretical Prediction of Roll Moments on Finned Bodies in Supersonic Flow***, AIAA Paper No. 74-111.

50. L. Frierson, ***Supersonic Aerodynamics of the 5-Inch RF Beamrider Guided Projectile***, NSWC/DL, Aerodynamics Memo No. DG-44-75-67, October 1975.

51. H. H. B. M. Thomas and B. F. R. Spencer, ***The Calculations of the Derivatives Involved in the Damping of the Longitudinal Short Period Oscillations of an Aircraft and Correlation With Experiment***, RAE Report No. Aero 2561, November 1955.

52. W. B. Kemp and R. E. Becht, ***Damping-In-Pitch Characteristics at High Subsonic and Transonic Speeds of Four 35° Sweptback Wings***, NACA RML53G29a, October 1953.

53. M. Tobak, ***Damping in Pitch of Low-Aspect-Ratio Wings at Subsonic and Supersonic Speeds***, NACA RMA52L04a, April 1953.

54. H. F. Emerson and R. C. Robinson, ***Experimental Wind Tunnel Investigation of the Transonic Damping-In-Pitch Characteristics of Two Wing-Body Combinations***, NASA Memorandum 11-30-58A.

55. M. Tobak, D. E. Reese, and B. H. Beam, ***Experimental Damping in Pitch of 45° Triangular Wings***, NACA RMA50J26, 1950.

56. B. H. Beam, ***The Effects of Oscillation Amplitude and Frequency on the Experimental Damping in Pitch of a Triangular Wing Having an Aspect Ratio of 4***", NACA RMA52G07, 1952.

57. L. C. MacAllister, ***The Aerodynamic Properties of a Simple Non Rolling Finned Cone-Cylinder Configuration Between Mach Numbers 1.0 and 2.5***", BRL Report No. 934.

58. I. Shantz and R. T. Groves, ***Dynamic and Static Stability Measurements of the Basic Finner at Supersonic Speeds***, NAVORD Report 4516, September 1960.

59. B. L. Uselton and J. C. Uselton, ***Test Mechanism for Measuring Pitch-Damping Derivatives of Missile Configurations at High Angles of Attack***, AEDC TR-75-43, May 1975.

60. E. B. O'Neill and K. A. Phillips, ***A Comparison of Damping-In-Pitch Derivatives Obtained Through Different Experimental Techniques***, Paper Presented at the 25th Semi-Annual Meeting of the Supersonic Tunnel Association, May 1966.

61. M. L. Robinson, ***The Estimation of Pitch Damping Derivatives of Missile Configurations at Subsonic Speeds***, AIAA Paper No. 70-537, May 1970.

62. D. G. Lee, ***A Survey of Methods for Estimating the Damping-In-Pitch Parameter***, NSRDC Report 2816, May 1968.

63. A. Braslow, H. Wiley, and C. Lee, ***A Rigidly Forced Oscillation System for Measuring Dynamic Stability Parameters in Transonic Wind Tunnels***, NASA TN-D-231, March 1962.

64. E. J. Ohlmeyer and T. R. Pepitone, ***Transonic Magnus Characteristics of Two Low Drag Projectile Configurations***, NWL TR-2586, November 1971.

65. R. H. Whyte, ***Effects on Boattail Angle on Aerodynamic Characteristics of 175mm M437 Projectile at Supersonic Mach Numbers***, PATM 1646, September 1965.

66. W. F. Donovan, ***Free-flight Range Tests of the 5"/38 Rocket Assisted Projectile (Inert)***, BRL MR 2071, November 1970.

67. E. D. Boyer, ***Aerodynamic Properties of the 90mm M-71 Shell***, BRL MR 1475, April 1963.

68. K. S. Krial and L. C. McAllister, ***Aerodynamic Properties of a Family of Shells of Similar Shape – 105mm XM 380E5, XM 380E6, T388 and 155mm T387***, BRL MR 2023, February 1970.

GLOSSARY OF TERMS

AR	Aspect ratio.
b	Wing span (does not include body radius).
c	Chord length at any point along span.
$\bar{c}$	Mean aerodynamic chord.
C_{D_0}	Zero lift drag coefficient.
C_ℓ	Rolling moment coefficient of wing planform.
c_ℓ	Local rolling moment coefficient.
C_{ℓ_P}	Roll damping moment coefficient $[C_\ell/(p\ell_{ref}/2V_\infty)]$.
C_M	Pitching moment coefficient measured about nose tip (positive nose up).
C_{M_α}	Pitching moment coefficient derivative $(dC_M/d\alpha)$.
$C_{M_Q} + C_{M_{\dot{\alpha}}}$	Total damping in pitch.
C_{M_Q}	Steady state damping in pitch $[(C_M)_q/(q\ell_{ref}/2V_\infty)]$.
$C_{M_{\dot{\alpha}}}$	Unsteady damping in pitch $[(C_M)_{\dot{\alpha}}/(\dot{\alpha}\ell_{ref}/2V_\infty)]$.
C_N	Normal force coefficient.
C_{N_α}	Normal force coefficient derivative $(dC_N/d\alpha)$.
$C_{n_{P_\alpha}}$	Magnus moment coefficient derivative.
$C_{y_{P_\alpha}}$	Magnus force coefficient derivative.
c_{N_P}	Sectional normal force coefficient derivative due to p motion.
c_{N_Q}	Sectional normal force coefficient derivative due to q motion.

$c_{N_{\dot{\alpha}}}$	Sectional normal force coefficient derivative due to $\dot{\alpha}$ motion.
C_P	Pressure coefficient.
(ΔC_P)	Difference in pressure coefficients of upper and lower surfaces of wing planform.
$(\Delta C_P)_p$	Difference in pressure coefficients of upper and lower surfaces of wing planform due to a rolling velocity, p.
$(\Delta C_P)_q$	Difference in pressure coefficients of upper and lower surfaces of wing planform due to a pitch rate q.
$(\Delta C_P)_{\dot{\alpha}}$	Difference in pressure coefficients of upper and lower surfaces of wing planform due to a constant vertical acceleration $\dot{\alpha}$.
d	Body diameter.
ℓ_{ref}	Reference length (body diameter for wing-body configuration).
ℓ_{BT}	Boattail length.
M	Mach number.
m	$\beta \cot \Lambda_1$.
n	Number of tail fins.
p	Roll rate.
q	Pitch rate.
q′	Dynamic pressure.
r_b	Body Radius.
r_n	Body nose radius.
S_w	Wing planform area.
u,v,w	Perturbation velocities in x_0, y_0, z_0 directions, respectively.

V	Total velocity.
x,y,z	Transformed coordinates.
x_0, y_0, z_0	Rectangular coordinate system with x at nose tip, y out right wing, and z positive up. If configuration consists of wing only, x begins at wing root chord.
x_a, y_a	Coordinates of wing tip.
α	Angle of attack.
β	$\sqrt{M^2 - 1}$.
δ	Canard deflection (degrees).
η	Howarth-Mangler variable.
θ_{BT}	Boattail angle.
Λ_i	Sweepback angle of a wing generator (i = 1,2,3,4) with i = 1, the wing leading edge, and i = 4 the wing trailing edge.
λ	Taper ratio.
σ	$\tan \Lambda_1 (y/x)$.
ω	Frequency of oscillation.

DISTRIBUTION

Commander
Naval Sea Systems Command
Washington, DC 20360
ATTN: SEA-03, Mr. Lionel Pasiuk
Technical Library (2)

Commander
Naval Material Command
Washington, DC 20360
ATTN: Mr. Sid Jacobson (MAT-032)
Dr. John Huth
Technical Library (2)

Commander
Naval Air Systems Command
Washington, DC 20360
ATTN: AIR-320, Mr. Bill Volz
AIR-320, Dr. H. Mueller
Technical Library (2)

Commander
Naval Weapons Center
China Lake, CA 93555
ATTN: Mr. Ray Van Aken
Mr. D. Meeker
Technical Library (2)

Commander
Pacific Missile Test Center
Point Mugu, CA 93041
ATTN: Mr. Joe Rom
Technical Library (2)

Commander
Naval Ship Research and Development Center
Washington, DC 20007
ATTN: Dr. T. C. Tai
Technical Library (2)

Commander
Naval Weapons Center
Corona Laboratories
Corona, CA 91720
ATTN: Technical Library (2)

Office of Naval Research
Pentagon
Washington, DC 20350
ATTN: Dr. R. J. Lundegard
Mr. Dave Seigel
Dr. Bob Whitehead
Mr. Mort Cooper
Mr. Ralph Cooper
Technical Library (2)

Officer in Charge
Carderock Laboratory
Naval Ship Research and Development Center
Bethesda, MD 20034
ATTN: Technical Library (2)

Deputy Chief of Naval Operations
(Development)
The Pentagon
Washington, DC 20350
ATTN: Technical Library (2)

Commanding Officer
Naval Air Development Center
Warminister, PA 18974
ATTN: Technical Library (2)

Commanding Officer
Naval Air Engineering Center
Aeronautical Structures Department
Lakehurst, NJ 19112
ATTN: Technical Library (2)

Chief of Naval Research
Department of the Navy
Washington, DC 20360
ATTN: Technical Library (2)

Commander
Pacific Missile Test Center
U. S. Naval Missile Center
Point Mugu, CA 93041
ATTN: Technical Library (2)

Director
Naval Strategic Systems Projects Office (PM-1)
Department of the Navy
Washington, DC 20360
ATTN: Technical Library (2)

Superintendent
U. S. Naval Academy
Annapolis, MD 21402
ATTN: Head, Weapons Department
Head, Science Department
Technical Library (2)

Superintendent
U. S. Naval Postgraduate School
Monterey, CA 95076
ATTN: Head, Mechanical Engineering Department
Head, Department of Aeronautics
Technical Library (2)

Officer in Charge
U. S. Naval Scientific and Technical Intelligence Center
U. S. Naval Observatory
Washington, DC 20360
ATTN: Technical Library (2)

Commanding Officer
Naval Ordnance Station
Indian Head, MD 20640
ATTN: Technical Library (2)

Commandant of the Marine Corps
Headquarters, Marine Corps
Washington, DC 20380
ATTN: Technical Library (2)

Director, Development Center
Marine Corps Development and Education Command
Quantico, VA 22134

Chief of S and R Division
Development Center
Marine Corps Development and Education Command
Quantico, VA 22134

Chief of Air Operations Division
Development Center
Marine Corps Development and Education Command
Quantico, VA 22134

Chief of Ground Operations Division
Development Center
Marine Corps Development and Education Command
Quantico, VA 22134

Marine Corps Liaison Officer
Field Artillery Board
Fort Sill, OK 73503
ATTN: Technical Library (2)

Commanding General
Ballistic Research Laboratory
Aberdeen Proving Ground, MD 21005
ATTN: Dr. C. H. Murphy
Mr. L. McAllister
Mr. A. Platou
Mr. B. McCoy
Technical Library (2)

Commanding General
Picatinny Arsenal
Dover, NJ 07801
ATTN: Mr. A. Loeb
Mr. Mertz
M. Cline
Technical Library (2)

Commanding General
U. S. Army Missile Command
Redstone Arsenal, AL 35809
ATTN: Mr. Ray Deep (DRSMI)
Dr. D. J. Spring (DRSMI)
Technical Library (2)

Commanding General
U. S. Army Material Command AMCRD-TP
Washington, DC 20315
ATTN: Technical Library (2)

Office of Chief of Research and Development
Washington, DC 20310
ATTN: Technical Library (2)

Commanding Officer
Army Chemical Center
Edgewood, MD 21040
ATTN: Technical Library (2)

Commanding General
Frankford Arsenal
Philadelphia, PA 19104
ATTN: Mr. W. Gadomski
Technical Library (2)

Commanding Officer
Harry Diamond Laboratories
Washington, DC 20013
ATTN: Technical Library (2)

Commanding Officer of U. S. Army Combat Development Command
Field Artillery Agency
Fort Sill, OK 73503
ATTN: Technical Library (2)

President of U. S. Army Field Artillery Board
Fort Sill, OK 73503
ATTN: Technical Library (2)

Aeronautical Research Laboratory
Wright-Patterson Air Force Base
Dayton, OH 45433
ATTN: Technical Library (2)

Aeronautical System Division
USAF
Wright-Patterson Air Force Base
Dayton, OH 45433
ATTN: Technical Library (2)

AF Office of Scientific Research
Washington, DC 20330
ATTN: Technical Library (2)

Arnold Engineering Development Center
USAF
Tullahoma, TN 37389
ATTN: Mr. J. Usselton
Mr. W. B. Baker, Jr.
Technical Library (2)

Headquarters, USAF
Systems Command
Andrews Air Force Base, MD 20331
ATTN: Technical Library (2)

Headquarters, USAF
Washington, DC 20330
ATTN: Technical Library (2)

Flight Research Center
Edwards Air Force Base, CA 93523
ATTN: Technical Library (2)

Air Force Rocket Propulsion Laboratory (AFSC)
Department of the Air Force
Edwards, CA 93523
ATTN: Major Washburn

U. S. Air Force Systems Command Regional Offices
c/o Department of the Navy
Washington, DC 20360
ATTN: Technical Library (2)

AFATL (ADLRA), (DLGC)
Eglin Air Force Base, FL 32542
ATTN: Dr. Daniel
Mr. C. Butler
Mr. C. Matthews
Mr. K. Cobb
Mr. E. Sears
Technical Library (2)

USAF Academy
Colorado Springs, CO 80912
ATTN: Technical Library (2)

Wright Air Development Center/AFFDL
Wright-Patterson Air Force Base, OH 45433
ATTN: Mr. E. Flinn (FGC)
Dr. G. Kurylowich (FGC)
Technical Library (2)

Applied Physics Laboratory
The John Hopkins University
8621 Georgia Avenue
Silver Spring, MD 20910
ATTN: Dr. L. L. Cronvich
Mr. Edward T. Marley
Dr. Gordon Dugger
Technical Library (2)

Advanced Research Projects Agency
Department of Defense
Washington, DC 20305
ATTN: Technical Library (2)

Director
Defense Research and Engineering
Department of Defense
Washington, DC 20305
ATTN: Technical Library (2)

George C. Marshal Flight Center
Huntsville, AL 35804
ATTN: Technical Library (2)

NASA Goddard Space Center
Greenbelt, MD 20771
ATTN: Technical Library (2)

NASA Lewis Research Center
Cleveland, OH 44101
ATTN: Technical Library (2)

NASA
Washington, DC 20546
ATTN: Technical Library (2)

NASA Ames Research Center
Moffett Field, CA 94035
ATTN: Mr. Vic Peterson
Mr. John Rakich
Technical Library (2)

NASA Langley Research Center
Langley Station
Hampton, VA 23365
ATTN: Mr. Bud Bobbitt
Mr. Jerry South
Mr. Leroy Spearman
Mr. C. M. Jackson, Jr.
Mr. W. C. Sawyer
Technical Library (2)

Virginia Polytechnic Institute and State University
Department of Aerospace Engineering
Blacksburg, Virginia 24060
ATTN: Prof. J. A. Schetz
Technical Library (2)

Stanford Research Institute
Menlo Park, CA 94025
ATTN: Dr. Milton Van Dyke
Technical Library (2)

Raytheon Company
Spencer Laboratory
Burlington, MA 01803
ATTN: Steve Pearlsing
Box SL 7162

North Carolina State University
Department of Mechanical and Aerospace Engineering
Box 5246
Raleign, NC 27607
ATTN: Prof. F. R. DeJarnette
Technical Library (2)

The University of Tennessee Space Institute
Tullahoma, TN 37388
ATTN: Dr. J. M. Wu
Technical Library (2)

Director Defense Research and Engineering
Department of Defense
Washington, DC 20301
ATTN: Bartley Osborne, R&AT Office

Dr. Jim Zerikos
McDonnell Douglas Astronautics Company (West)
5301 Bolsa Avenue
Hunington Beach, CA 92647
Mall Station 13-2

Mr. B. H. Shirley
Lockheed Missiles & Space Co., Inc.
P. O. Box 1103, W. Street
Huntsville, AL 35807

Dr. Lars E. Erisson
Lockheed Missiles & Space Co., Inc.
Department 81-10, Bldg. 154
Sunnyvale, CA 94088

Nielsen Engineering and Research, Inc.
510 Clyde Avenue
Mountain View, CA 94043

Mr. V. L. Pianta
Senior Project Engineer
P. O. Box 1201
San Jose, CA 95108

Defense Documentation Center
Cameron Station
Alexandria, VA 22314 (12)

Library of Congress
Washington, DC 20390
ATTN: Gift and Exchange Division (4)

Defense Printing Service
Washington Navy Yard
Washington, DC 20374

Local:

DG
DG-10 (Swanson) (10)
DG-44 (6)
DK
DK-20
DK-21 (40)
DK-50

DX-21 (2)
DX-222 (6)
DX-40
DX-43 (Elliott)
WA
WA-20 (Mr. B. Piper)
WA-20 (Mr. G. Graff)
WÁ-30
WA-40
WA-40 (Mr. F. Regan)
WA-40 (Mr. S. Hastings)
WA-40 (Dr. J. Goeller)
WA-40 (Dr. N. Sheetz)
WA-40 (Dr. J. Solomon)
WA-40 (Mr. F. Baltakis)
WA-50
WR